



**ANALYSIS OF THE PUNCHING PROCESS OF
AZ31 ALLOY SHEET WITH EXPERIMENTAL
AND SIMULATION STUDIES**

**2022
MASTER THESIS
MECHANICAL ENGINEERING**

Fadell Said Ahmed ABOSHBA

**Thesis Advisor
Prof. Dr. Bilge DEMİR**

**ANALYSIS OF THE PUNCHING PROCESS OF AZ31 MG ALLOY SHEET
WITH EXPERIMENTAL AND SIMULATION STUDIES**

Fadell Said Ahmed ABOSHBA

**T.C.
Karabuk University
Institute of Graduate Programs
Department of Mechanical Engineering
Prepared as
Master Thesis**

**Thesis Advisor
Prof. Dr. Bilge DEMİR**

**KARABUK
February 2022**

I certify that in my opinion the thesis submitted by Fadell Said Ahmed ABOSHBA titled " ANALYSIS OF THE PUNCHING PROCESS OF AZ31 MG ALLOY SHEET WITH EXPERIMENTAL AND SIMULATION STUDIES " is fully adequate in scope and quality as a thesis for the degree of Master of Science.

Prof. Dr. Bilge DEMİR

.....

Thesis Advisor, Department of Mechanical Engineering

This thesis is accepted by the examining committee with a unanimous vote in the Department of Mechanical Engineering as a Master of Science thesis. 24.02.2022

Examining Committee Members (Institutions)

Signature

Chairman : Doç. Dr. Hakan GÜRÜN (GÜ)

.....

Member : Prof. Dr. Bilge DEMİR (KBÜ)

.....

Member : Dr. Öğr. Üyesi Gökhan SUR (KBÜ)

.....

The degree of Master of Science by the thesis submitted is approved by the Administrative Board of the Institute of Graduate Programs, Karabuk University.

Prof. Dr. Hasan SOLMAZ

.....

Director of the Institute of Graduate Programs

"I declare that all the information within this thesis has been gathered and presented in accordance with academic regulations and ethical principles and I have according to the requirements of these regulations and principles cited all those which do not originate in this work as well."

Fadell Said Ahmed ABOSHBA

ABSTRACT

M. Sc. Thesis

ANALYSIS OF THE PUNCHING PROCESS OF AZ31 MG ALLOY SHEET WITH EXPERIMENTAL AND SIMULATION STUDIES

Fadell Said Ahmed ABOSHBA

**Karabük University
Institute of Graduate Programs
The Department of Mechanical Engineering**

Thesis Advisor:

Prof. Dr. Bilge DEMİR

February 2022, 70 pages

AZ31 magnesium alloy is a widely-used aluminium-magnesium alloy in the aerospace industry to produce flat components. Punch punching is one of the most common processes used in automobile manufacturing; However, it is an essential and straightforward procedure in terms of business. It is necessary for high-quality products and helps manufacture high-quality and complex products. That is why researchers have conducted many studies on it. Some factors such as punching clearance, punching force, punching speed, empty holder force, and punching tip geometry are the basic parameters that determine the punching product quality. The punching tip shape is the most critical component, significantly affecting the cutting force.

This thesis investigates the punch ability of AZ31 magnesium sheets using different punch bits under standard conditions. If we take a closer look, the punching process

uses various punch ends. This thesis discusses the part failure analysis and punch-shape evaluation, which are significant for cutting and punch quality. For this research, we created a simplified simulation model for experimentation using a digital-to-analogue converter, which primarily transmits the amplified signal to the computer. Three different punch heads were used (0, R, and 16). This research shows that punching force is much higher when we perform punching using a punch with the angular opening of P1 as compared to P2 and P3 punches.

This study examined the punching surfaces formed due to experimental studies with the help of a digital microscope and Scanning Electron Microscope (SEM). P1 produced higher quality punched holes and attained burr heights just in 1.08s. The original profile of the cutting edge remained suitable for high-quality holes, which is evident from ignorable weight loss. Through 3D simulation, the researcher determined the critical damage constant for Mg AZ31 alloy. Three punches were P1, P2, and P3 with geometrical compressions P1, P2, and P3.

Flat and P3 punches created the most uniform cutting surfaces. Correspondingly, we observed the lowest punching forces from the P3 punch. Experimental and finite element analyses show that punching forces decrease because of the surface cutting angle in P1, P2, and P3 punches. Different punch geometries affect the stress distribution and fracture formation on the workpiece. It is a fact that punch tip surface area affects the punch force with fewer time limitations. The three punching experiments, including P1, P2, and P3, were performed using the finite element method. The reference force values matched the force values obtained from the experimental techniques. P1 (0) showed a good cutting surface and no damage; P1 showed better performance than P2. Punching experiments with three different geometries showed that the highest punch force occurred in the P1(0) punch experiments. In contrast, the lowest punch forces occurred in the experiments with the P3 punch.

Keywords : Punching, Magnesium AZ31 Alloy, Punch Tips. Tensile Test, Magnesium AZ31 Microstructure.

Science Code: 91421, 91438

ÖZET

Yüksek Lisans Tezi

AZ31 MG ALAŞIM SACININ ZIMBA İLE DELME İŞLEMİNİN DENEY VE SİMÜLASYON ÇALIŞMALARI İLE ANALİZİ

Fadell Said Ahmed ABOSHBA

Karabük Üniversitesi

Lisansüstü Eğitim Enstitüsü

Makina Mühendisliği Anabilim Dalı

Tez Danışmanı:

Prof. Dr. Bilge DEMİR

Şubat 2022, 70 sayfa

AZ31 magnezyum alaşımı, havacılık endüstrisinde yassı bileşenler üretmek için yaygın olarak kullanılan bir alüminyum-magnezyum alaşımıdır. Punch delme, otomobil üretiminde kullanılan en yaygın işlemlerden biridir, ancak iş açısından temel ve basit bir prosedür olmasına rağmen, yüksek kaliteli ürünler için gereklidir ve yüksek kaliteli ve karmaşık ürünlerin üretilmesine yardımcı olur. Bu nedenle araştırmacılar bu konuda birçok çalışma yapmışlardır. Delme boşluğu, delme kuvveti, delme hızı, boş tutucu kuvveti ve delme ucu geometrisi gibi bazı faktörler, delme ürün kalitesini belirleyen temel parametrelerdir. Delme ucunun şekli, kesme kuvvetini önemli ölçüde etkileyen en kritik bileşendir.

Bu tez, standart koşullar altında farklı zimba uçları kullanan AZ31 magnezyum levhaların zımbalama kabiliyetini araştırmaktadır. Daha yakından bakarsak, zımbalama işlemi çeşitli zimba uçları kullanır. Bu tez, kesme ve zimba kalitesi için

önemli olan parça arıza analizi ve zımba şekli değerlendirmesini tartışır. Bu araştırma için, öncelikle güçlendirilmiş sinyali bilgisayara ileten bir dijital-analog dönüştürücü kullanarak deney için basitleştirilmiş bir simülasyon modeli oluşturduk. Zımbalama işleminde üç farklı zımba kafası (0, R ve 16) kullanılmıştır. Bu araştırma, P1'in açılal açıklığına sahip bir zımba kullanarak zımbalama yaptığımızda zımbalama kuvvetinin P2 ve P3 zımbalara kıyasla çok daha yüksek olduğunu göstermektedir.

Bu çalışmada ayrıca dijital mikroskop ve Taramalı Elektron Mikroskobu (SEM) yardımıyla deneysel çalışmalar sonucunda oluşturulan delme yüzeyleri incelenmiştir. Sonuçlar, P1'in daha yüksek kalitede zımbalanmış delikler ürettiğini ve sadece 1.08 saniyede çapak yüksekliklerine ulaştığını gösterdi. Kesici kenarın orijinal profili, yüksek kaliteli delikler için uygun kaldı. Araştırma, 3D simülasyon yoluyla Mg AZ31 alaşımı için kritik hasar sabitini tanımladı. Üç zımba, sırasıyla P1, P2 ve P3 geometrik sıkıştırma seviyelerine sahip P1, P2 ve P3 idi. Düz ve P3 zımbalar, en düzgün kesme yüzeylerini oluşturdu. Buna uygun olarak, P3 zımbadan en düşük zımbalama kuvvetlerini gözlemledik. Deneysel ve sonlu eleman analizleri de P1, P2 ve P3 zımbalarda yüzey kesme açısı nedeniyle zımbalama kuvvetlerinin sırasıyla azaldığını göstermektedir. Farklı zımba geometrileri, iş parçası üzerindeki gerilim dağılımını ve kırılma oluşumunu etkiler. Zımba ucu yüzey alanının daha az zaman sınırlaması ile zımba kuvvetini etkilediği bir gerçektir. P1, P2 ve P3 dahil olmak üzere üç delme deneyi, sonlu elemanlar yöntemi kullanılarak gerçekleştirilmiştir. Referans kuvvet değerleri, deneysel tekniklerden elde edilen kuvvet değerleriyle eşleşti. P1 (0) iyi bir kesme yüzeyi gösterdi ve hasar yok; P1, P2'den daha iyi performans gösterdi.

Anahtar Kelimeler : Punching, Magnesium AZ31, Punch Tips. Tensile test, Magnesium AZ 31.

Bilim Kodu : 91421, 91438

ACKNOWLEDGMENT

First, I sincerely and whole-heartedly thank my advisor, Prof. Dr. Bilge DEMIR, for his efforts and support, and I value his knowledge. I also acknowledge the great help and support of Khalil Belras Ali (Karabuk University), Doç Dr. Hakan Gürün (Gazi University), and the university staff.

I also value the help and support of my parents, sisters, brothers, and friends for their kind support during my learning period. I extend my sincerest love to my mother and wife for their contributions to my life and career, and I value their moral support during my academic career.

CONTENTS

	<u>Page</u>
APPROVAL.....	ii
ABSTRACT.....	iv
ÖZET.....	vi
ACKNOWLEDGMENT.....	viii
CONTENTS.....	ix
LIST OF FIGURES.....	xii
LIST OF TABLES.....	xvi
SYMBOLS AND ABBREVIATIONS.....	xvii
PART 1.....	1
INTRODUCTION.....	1
1.1. HISTORY.....	3
1.2. AZ31 MAGNESIUM SHEET/PLATE.....	4
1.3. MECHANICAL BEHAVIOR OF AZ31 ALLOYS.....	5
1.4. PROBLEM STATEMENT.....	5
1.5. OBJECTIVES OF THE STUDY.....	6
1.6. AIM OF THIS WORK.....	6
1.7. THESIS ORGANIZATION.....	6
PART 2.....	7
LITERATURE REVIEW.....	7
2.1. MAGNESIUM CHARACTERISTICS.....	7
2.2. ALLOY DESIGNATIONS.....	9
2.3. AZ31.....	11
2.4. MECHANICAL PROPERTIES.....	12
2.5. FORMABILITY OF MAGNESIUM ALLOYS.....	13
2.5.1. Formability of AZ31 MG Alloy Sheets.....	13
2.5.2. Shearing Process for AZ31 Magnesium Alloy.....	16

	<u>Page</u>
2.6. MAGNESIUM APPLICATIONS	18
2.6.1. Magnesium Application in Aerospace Industries.....	18
2.7. ADVANTAGES AND DISADVANTAGES OF AZ31	19
2.7.1. Advantages of AZ31	19
2.7.2. Disadvantages of AZ31	19
2.8. EFFECTS OF SHEAR-DAMAGED AREA ON MAGNESIUM ALLOY AZ31	20
2.9. VARIOUS HOLE EXPANSION MAGNESIUM ALLOYS	21
2.10. ANGULAR STRETCH BEND MG AZ31	22
 PART 3	 24
SHEET METAL FORMATION.....	24
3.1. PUNCHING (PIERCING AND BLANKING).....	24
3.1.1. Sheet Metal Punching Process.....	26
3.1.2. Punching Operation	26
3.1.3. Die Clearance.....	27
3.1.4. Hydraulic Punch Press.....	28
3.2. RELATED STUDIES	29
 PART 4	 32
EXPERIMENTAL AND THEORETICAL ANALYSIS	32
4.1. MATERIALS	33
4.2. TENSILE TEST	33
4.3. PUNCH GEOMETRIES AND PUNCHING PROCESS	35
4.4. PERFORMING PUNCHING PROCESSES WITH FINITE ELEMENT METHOD	38
4.5. MEASUREMENT OF THE DIMENSIONS OF PUNCHED PARTS.....	40
4.5.1. Punched Part Images and Failure Analysis	40
 PART 5	 42
RESULTS AND DISCUSSION	42
5.1. TENSILE TEST	42
5.1.1. Tensile Test and Fracture Mode	42

	<u>Page</u>
5.1.1.1. Tensile fracture mode.....	45
5.2. INVESTIGATION OF THE CUTTING FORCES THAT OCCURRED DURING THE PUNCHING PROCESS.	46
5.2.1. Shear Force Analysis with FEM Software	48
5.3. MEASUREMENT OF THE DIMENSIONS OF PUNCHED PARTS.....	51
5.3.1. Dimensional Analysis of Holes Created by the Punching Test.....	51
5.3.2. Diameter Deviations and Deviation from Circularity (Ovality).....	54
5.3.3. Investigation of Cutting Surfaces Resulting from Punching Process by A Digital Microscope	55
5.3.4. Investigation of Cutting Surfaces Resulting from Punching Process by Using SEM	58
 PART 6	 61
CONCLUSIONS.....	61
 REFERENCES.....	 63
 RESUME	 70

LIST OF FIGURES

	<u>Page</u>
Figure 1.1. Plane pole figures of rolled AZ31 and Mg 1.5Zn-0.2Ce alloy sheets.....	2
Figure 1.2. Brackets used in the aircraft industry	4
Figure 2.1. Magnesium (Mg), an alkaline-earth metal of Group IIa of the Periodic Table.....	8
Figure 2.2. Magnesium alloy	9
Figure 2.3. Examples of magnesium alloy usage in Boeing 747: seat and wing components.....	11
Figure 2.4. Broken magnesium conical cups obtained from various experiments....	15
Figure 2.5. Conventional shearing process phases	16
Figure 2.6. Comparison of typical sheared edge profiles at various AZ31 magnesium alloy temperatures: (a) 100°C (b) 200°C, (c) 300°C and (d) 400°C	17
Figure 2.7. Fracture in magnesium AZ31 (a) A primary rough fracture is shown on the side; (b) The profile of the secondary curved fracture is shown on the side.....	21
Figure 2.8. Average value influence on highest degree of stress and bending radius	22
Figure 3.1. Blanking operation in sheet metal	25
Figure 3.2. Punching operation in sheet metal	25
Figure 3.3. The force-time curve for sheet metal blanking and punching.....	27
Figure 3.4. Die clearance definition	28
Figure 3.5. The appearance of a cut edge	28
Figure 3.6. Hydraulic punch press.....	29
Figure 3.7. The layout of the hydraulic punch press	29
Figure 4.1. Experimental flow chart.....	32
Figure 4.2. Microstructure of the used AZ31 alloy.	33
Figure 4.3. Tensile test samples of Mg AZ31 alloy.	34
Figure 4.4. Dimensions of standard tensile test samples.	34
Figure 4.5. Dimensions of Mg AZ31 alloy samples for tensile test.....	35
Figure 4.6. Experimental setup of punch-die with samples.....	36
Figure 4.7. Schematic assembly of a punch test.....	37

	<u>Page</u>
Figure 4.8. Schematic assembly of a punch test.	37
Figure 4.9. Mg AZ31 sample sheet.	39
Figure 4.10. Experimental test based on punching processes P1, P2, and P3.	39
Figure 4.11. Dimensions: Thickness 3mm, length 151.26mm, and width 27 mm. ...	40
Figure 4.12. Dimensions for all punches P1, P2, and P3 (20mm).	40
Figure 4.13. Punched and cut part	41
Figure 4.14. Flowchart of damage analysis.	41
Figure 5.1. A-C. Mg AZ31 alloy microstructure.	43
Figure 5.2. Tensile test and fracture mode.	44
Figure 5.3. Engineering true Stress-Strain Curve for Mg AZ31 alloy.	44
Figure 5.4. Tensile test measurement after the test.	45
Figure 5.5. The tensile fracture mode of Mg AZ31 alloy.	45
Figure 5.6. Mg AZ31 alloy cutting forces derived from punching for all punch geometries.	46
Figure 5.7. P1 (0°) flat punch versus P2(R).	47
Figure 5.8. P1 (0°) flat punch versus P3 (16°) punch cutting force.	48
Figure 5.9. Results were obtained using the 3D model for punching P1 (0°) and P2 (R) punches of Mg AZ31 alloy.	49
Figure 5.10. Results were obtained after using the 3D model for punching P3 (16°) punches of Mg AZ31 alloy.	49
Figure 5.11. P1 (0°) straight punch and P2 (R) punch analysis and experimental study of cutting forces.	50
Figure 5.12. P3 (16) punch analysis and experimental study of cutting forces.	50
Figure 5.13. Comparison between cutting forces from FEM and punching operations for Mg AZ31 alloy.	51
Figure 5.14. Dimensions of punch geometry (length 151.26mm, width 27mm).	51
Figure 5.15. Dimensions of punches P1 (0°), P2(R), and P3 (16°).	51
Figure 5.16. Hole diameters formed based Mg AZ31 sheet metal's punch geometry	52
Figure 5.17. Blanking diameters formed according to Mg AZ31 sheet metal's punch geometry.	53
Figure 5.18. Diameter deviation for Mg AZ31 alloy punch geometry of the hole. ...	54
Figure 5.19. Diameter deviation for MgAZ31 alloy punch geometry for blanking. .	54
Figure 5.20. Deviation from the circularity of the hole (workpiece) and blanking punch geometry.	55
Figure 5.21. The cutting surface of Mg AZ31 alloy for all punch geometries.	57

LIST OF TABLES

	<u>Page</u>
Table 2.1. A Common alloy according to standard ASTM alloy identification system	10
Table 2.2. Elements of AZ31	12
Table 4.1. Chemical composition of the used AZ31 Mg alloys.....	33
Table 5.1. MgAZ31 alloy cutting surface image formed after drilling with a punch.	56
Table 5.2. Rollover depth, burnish depth, fracture depth, and burr height.	57
Table 5.3. Cutting surface images of Mg AZ31 taken by SEM.....	58
Table 5.4. Side profile shapes of falling parts were obtained by using different punches	59
Table 5.5. Side profile shapes of the falling parts were obtained by using different punches.	60

SYMBOLS AND ABBREVIATIONS

ABBREVIATIONS

Al	: Aluminium
Cu	: Copper
Fe	: Iron
ND	: Normal Direction
Ni	: Nicle
TRC	: Twin-Roll Casting
Zn	: Zinc

PART 1

INTRODUCTION

Magnesium alloys are used for sophisticated industrial applications because they are strong and have excellent resistance to electromagnetic interference. Moreover, magnesium is the second most widely utilized mineral on our planet after zinc [1]. For lightweight transportation applications, magnesium alloys are used, which generally reduce greenhouse gas emissions and reduce the cost of transportation fuels. Besides, fuel consumption in automobile power trains has focused chiefly on magnesium alloys [2].

Magnesium alloys are magnesium mixtures, and magnesium is a light structural metal, and it forms alloys with other metals, including zinc, aluminium, silicon, manganese, rare earth, copper, zirconium, and copper. Additionally, most magnesium alloys have hexagonal lattice structures that affect the alloy's fundamental properties. In addition, the mentioned hexagonal lattice structure undergoes plastic deformation, which is more complex than cubic-latticed alloys, such as Mg alloy AZ31, steel, and copper alloys; so, magnesium alloys act like cast alloys. Since 2003, researchers have conducted extensive research on wrought alloys. Similarly, cast magnesium alloys help manufacture modern automobile components and high-performance vehicles.

Furthermore, magnesium alloys are the lightest available options in the alloy market. It is the sixth most popular alloy, extensively used in mechanical, automotive, and other industrial applications [3].

After World War II, extensive use of magnesium alloy started in the defense and aircraft manufacturing industries. In the same way, it is still used in the automotive industry today, especially in sandblasting and castings. Many experts have proposed magnesium alloys as a possible alternative to even high-strength steel [4].

Magnesium alloys, including AZ31, AZ80, and AZ61, are beneficial when strength is required because that justifies their high costs [1]. Some previous studies have shed light on the formability of magnesium alloy sheets, which is their main feature. Plastic deformation generates heat during the formation process. It is lost through radiation, convection, and conduction. The environment in which the alloy is processed changes the workpiece properties. Thus, accurate methods are needed to investigate the magnesium alloy formation. It is not just because of the deformation but also because of heat transfer. For this purpose, the Finite Element Method (FEM) is a suitable and effective method for simulating modulation and accurate deformation prediction. Similarly, FEM is helpful for analysis and designing the estimated optimal conditions for formation processes. In addition to the study, FEM is suitable for optimum estimated conditions for the formation operation [5-7]. One of the studies on warm deep drawing shows how imposing a thermal gradient in the open center helps. It remained in contact with the blank edge and the hole.

When the researchers used this technique, the specific drawing ratio of Mg alloy significantly improved. Particularly, temperature modulation was emphasized based on the edge and the open center [8]. Other studies have also been conducted based on the shear punch test (SPT) and single tensile test. They evaluated different mechanical properties of AZ31 [9]. In the same way, the study shows base texture (0002) of AZ31 alloys Mg-3Al-1Zn (mass %) and Mg-1.5Zn-0.2Ce (mass %) alloys as hot-rolled with the same rolling procedure as Figure 1.1 shows [10].

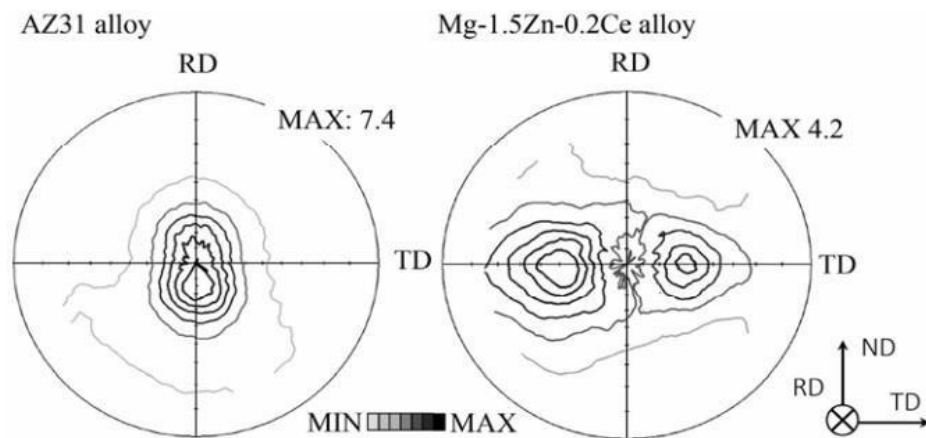


Figure 1.1. Plane pole figures of rolled AZ31 and Mg 1.5Zn-0.2Ce alloy sheets [10].

There are a few studies on the punching processes of magnesium alloys in the literature search. However, no study has been found on the punching processes of grade AZ31 Mg alloy. Therefore, the academic need for this study was understood, and this study was organized. AZ31 magnesium alloy, widely used commercially, was preferred in the study. Different punches were used in the experiments. This was because the effect of flat punch and different angle and shaped punch tips on cutting forces and cutting surface quality were quite high in the literature study. The punching surfaces formed in the parts resulting from experimental studies were examined with the help of a digital microscope and Scanning Electron Microscope (SEM). Also, the critical damage constant for Mg AZ31 alloy was investigated through 3D simulation. Different punch geometries affect the stress distribution and fracture formation on the workpiece. It is a fact that the punch tip surface area affects punch force with less time constraint. Three punching experiments, including P1, P2 and P3 coded, were performed using the experimental and finite element method. The reference force values were matched with the force values obtained from the experimental techniques. P1 (0) showed a good cutting surface and no damage; P1 performs better than P2. As a result, punching cutting forces and surface quality with different punch tips were examined in detail in terms of quantity and quality.

1.1. HISTORY

Among the structural metals, magnesium is the lightest, and its density is 1.74g/cm^3 in a solid-state. Magnesium's physical and mechanical characteristics help manufacture engineering products [11]. Furthermore, magnesium and its alloys offer several advantages because it is 75% lighter than steel and 33% lighter than the Mg alloy AZ31, which means that it has the lowest density compared to any other commercial casting alloy. Magnesium alloys have a comparable strength-to-weight relationship despite their lower density.

Magnesium is a bright and silver-white alkaline metal of the earth [12,13] with terrestrial and cosmic abundances, and it is highly reactive, so it is never found free [14]. Joseph Black (1754) identified it, and Friedrich Hoffmann (1729) made contributions to its development [15]. Furthermore, magnesium has played an essential

part in the evolution of civilization. Early military applications and the need for combat equipment were the driving force behind its growth. For example, experts used it for manufacturing incendiary bombs, flashlights, and ammunition used during the Second World War [16].

There are many types of magnesium, including AZ31, which performs for automotive, aerospace, and automotive engineering applications, and besides, some manufacturers add it to organic chemicals [17]. Moreover, it helps general applications, including household goods, office equipment, and sports equipment [16]. AZ31 has potential in aircraft manufacturing because of its mechanical properties and low density [18].

Aircraft designing branches witnessed substantial technique developments, which increased the demand to develop materials with low specific gravity. Furthermore, manufacturers fulfilled the requirements and orders using magnesium alloys. AZ31 magnesium alloys helped improve the aircraft industry because of their features, including good plasticity [19]. They are specifically used to manufacture parts with small loads, such as brackets to control an aircraft's flying tools. In addition, shelf manufacturing using magnesium alloys decreases the overall aircraft weight and reduces the total fuel consumption. In the case of ribs, the destination determines the number and shape of ribs in the brackets, as Figure 1.2 shows.

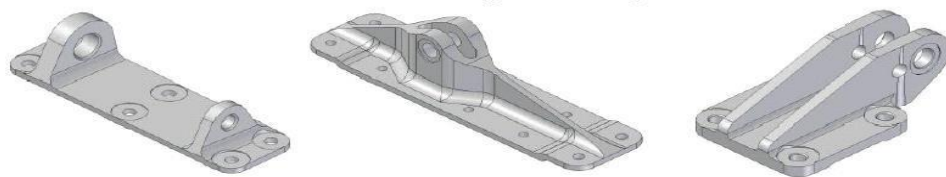


Figure 1.2. Brackets are used in the aircraft industry [18].

1.2. AZ31 MAGNESIUM SHEET/PLATE

Magnesium alloys have gained great importance, and they are much lighter than the metal structure materials for engineering applications. As mentioned above, magnesium alloys help manufacture automobiles, weapons, aircraft, and electronic

equipment because of their high strength, low density, sound damping features, and stiffness. In the aircraft industry, magnesium alloys have replaced many metals, for instance, steel, iron, and alloys, because they decrease the weight of planes, which contributes to reducing the overall fuel consumption, which also decreases the total CO₂ emissions. Magnesium alloys are four times lighter than steel, and the AZ31 alloy is the most common and ductile amongst AZ-shaped alloys.

This soft alloy combines flexibility and strength that makes it useful for structural applications. The AZ31 alloy wrought magnesium tooling plate offers many advantages and unique features that give AZ31 several benefits, such as vibration absorbance for longer life, stability of dimensions, and a longer tooling age (4 to 5 times). Additionally, the magnesium sheet and plate AZ31 alloy benefit many applications with medium strength service at temperatures below 150C [20].

1.3. MECHANICAL BEHAVIOR OF AZ31 ALLOYS

Magnesium and its alloys are attractive options because of their lightweight structural applications in aerospace and automobile manufacturing [11,21]. They are popular because they have a low density and a high strength-to-weight ratio. Good machinability, easy availability, and good castability are other beneficial features. But, poor flexibility, poor cold workability, and low strength limit their application [21]. Traditionally, Al, Zn, Mn, Ca alloys enhance the Mg-based materials' mechanical properties.

1.4. PROBLEM STATEMENT

As mentioned before, AZ31 is a widely-utilized aluminium-magnesium alloy, which offers a great deal of hope to the aviation sector because of its outstanding mechanical properties; however, just a few studies discuss it. This study investigates the application areas and mechanical and metallurgical properties of AZ31 with different punch tips. Through this study, some material constants will be defined, for instance, Analysis of the punching process of AZ31 Mg alloy sheet with experimental and simulation studies.

1.5. OBJECTIVES OF THE STUDY

- To study a Analysis of the punching process of AZ31 Mg alloy sheet with experimental and simulation studies.
- To review the chemical and mechanical properties of AZ31 and their relationship to the alloy forming process.
- The fourth part presents simulations of the perforating process using FEM and some mechanical tests performed on the Mg AZ31 alloy sheet metal used in the experimental part of this study.
- The effects of the geometry of different punching processes on cutting strength, hole diameter dimensions, precision, and cutting surface quality in perforating Mg AZ31 alloy sheet materials were investigated.
- Finally, the experimental section deals with the FEM process simulation results for Mg AZ31 alloy sheets and various mechanical tests performed on the metal used in the practical part of this study.

1.6. AIM OF THIS WORK

The aim is to analyze the mechanical and metallurgical properties of AZ31 through theoretical and experimental investigation of the punching process. For this purpose, the researcher has applied diverse punch tips and examined mechanical properties and internal structure.

1.7. THESIS ORGANIZATION

The organization of this work comprises the following six chapters:

The organization of this work comprises the following six chapters: Chapter 1: Introduction, Chapter 2: Literature Review, Chapter 3: Theoretical Analysis, Chapter 4: Research Methodology, Chapter 5: Results and Discussion, Chapter 6: Conclusion and Recommendations .

PART 2

LITERATURE REVIEW

High strength-to-weight magnesium alloys contain magnesium, rare earth, manganese, zinc, zirconium, and thorium, which are significant for applications and situations in which a decrease in weight is vital, and the strength of inertia is necessary. Some dense materials, including cast iron, steel, or copper-base alloys, on the other hand, have been replaced with Mg-based alloys. Magnesium was initially used (22kg) in Beetle by the Volkswagen Car Company [22].

2.1. MAGNESIUM CHARACTERISTICS

In the periodic table with the symbol Mg, magnesium is in Group II, as Fig. 2.1 indicates. Pure magnesium has the lowest ambient temperature among the available metals and 1.745g/cm density. In the same way, pure magnesium has no strength to make it considerable for structural construction. The addition of metals to form an alloy with, for example, zinc (Zn) or aluminium (Al) improves this condition. As mentioned before, Mg alloy AZ31 gives the finishing alloy substantial additional strength and stiffness and helps smooth casting when the alloy's full freezing range expands [23].

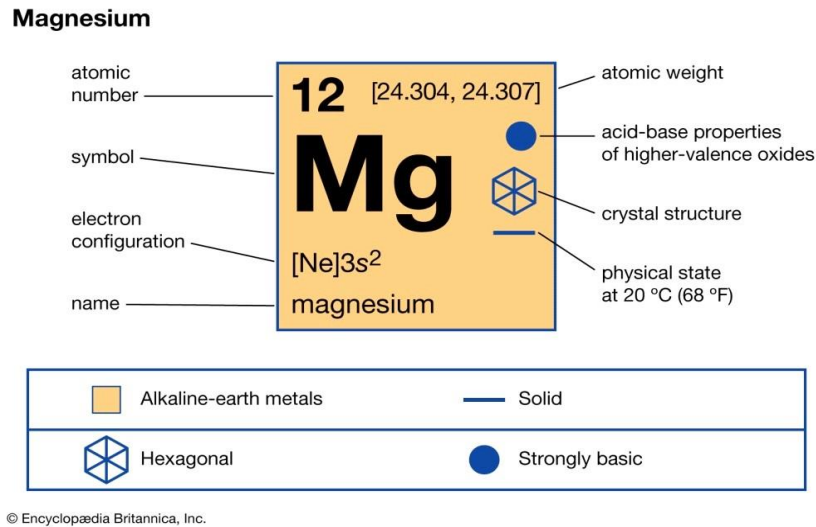


Figure 2.1. Magnesium (Mg) is an alkaline-earth metal of Group IIa of the periodic table [25].

China processes 85% of the total magnesium and uses the Pidgeon method, an inexpensive alternative to the electrolytic process in Canada in the 1940s. At 1000–1300°C, manufacturers calcinate crushed Mg ore (dolomite) through the mentioned Pidgeon process. It yields the required dolomite (CaO•MgO), and an arc furnace crushes it at 1600°C and mixes it with ferrosilicon, an iron alloy. It is possible to obtain silicon from coke, silica sand, and iron scrap [22,24].

Zinc added to the magnesium alloy enhances its room temperature resistance and corrosion resistance to contaminants, for instance, iron and nickel. Manganese reduces its corrosive capacity in the alloy. In the chemical composition of the alloy, there is a limited need for manganese.

In the same way, the environment can be highly corrosive, specifically when it comes in contact with water. The hardness of magnesium alloys enhances by using silver. In most alloying components, experts extensively use silicon. In Mg alloys, its principal purpose is molten metal fluidity. It also creates cracking resistance in the alloy because it creates Mg₂Si particles attached to the grain limits. Rare-earth element reduces porosity and cracks in the Mg alloy because it decreases the alloy's freezing range [23].

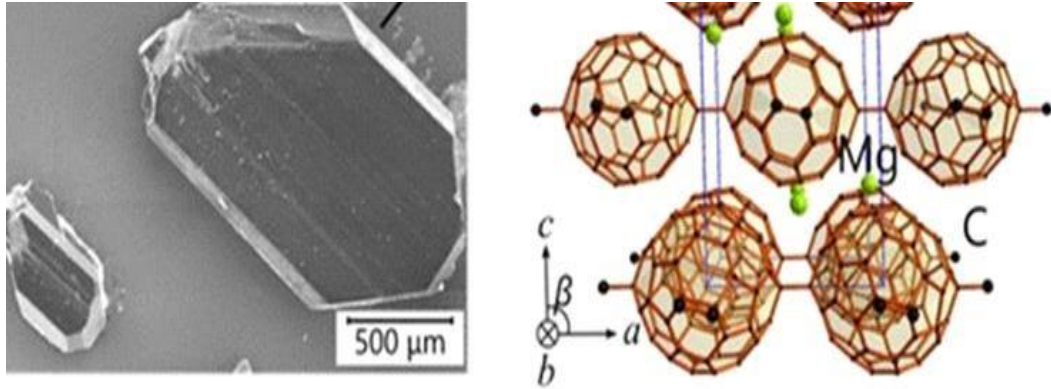


Figure 2.2. Magnesium alloy [25].

When combined with other metallic elements, pure magnesium improves its properties and maintains them even at a high temperature; for example, in AZ31, silicon, zinc, zirconium, rare earth metals, and copper are combined. The mentioned reasons show that Mg alloys are beneficial for aerospace, manufacturing, automobile, and mechanical industries. If the three main vehicle components (powertrain, chassis, and body) replace with Mg alloys, it reduces the overall vehicle weight by 20-70%. Moreover, magnesium alloys show excellent heat dissipation and vibration damping properties, essential for many industries. Vibration affects car efficiency, but Mg alloys reduce it [25].

2.2. ALLOY DESIGNATIONS

There is frequent use of designation systems to characterize the chemical composition of an alloy system or a single alloy. Although there are other such systems, experts prefer the ASTM Standard Alloy Designation System (B951-11) for scientific publications, and this study has also used the same approach. There are four sections in the ASTM Standard Alloy Designation System; the first part is the main alloy elements defined in one letter, while the second has various rounded-off constituents' weight percentages. The third and fourth components include the standardizing number (from letters A through O and I) and the designation of the temperature [26].

Unfortunately, ASTM does not show all accessible alloying elements, so this paper adopts designations utilized by the cited authors. Table 1 reviews the alloying

components and their relevant ASTM-based assignments. Table 2.1 shows their temperature designations [26].

Table 2.1. Common alloy designations according to the standard ASTM alloy identification system [26].

Element			Element		
Designation	Name	Abbrev.	Designation	Name	Abbrev.
A	Aluminium	Al	N	Nickel	Ni
B	Bismuth	Bi	P	Lead	Pb
Ba	Barium	Ba	Q	Silver	Ag
C	Copper	Cu	R	Chromium	Cr
D	Cadmium	Cd	S	Silicon	Si
E	Rare earth	RE/REE	T	Tin	Sn
F	Iron	Fe	V	Gadolinium	Gd
H	Thorium	Th	W	Yttrium	Y
J	Strontium	Sr	X	Calcium	Ca
K	Zirconium	Zr	Y	Antimony	Sb
L	Lithium	Li	Z	Zinc	Zn
M	Manganese	Mn			

The casting magnesium alloys include alloying elements: Mag alloy AZ31, manganese, zinc, rare earth, and zirconium. Manufacturers commercially manufacture them (and as investments as well). The following categories of the mentioned alloy systems exist in the alloy families (magnesium-zinc-manganese-aluminium) [26].

- Magnesium-rare earth-zinc-zirconium (ZK, ZE)
- Magnesium-zirconium-rare earth (WE)
- Magnesium-zirconium-rare earth-silver (EZ, EQ, EK, EV)

2.3. AZ31

Portevin and DE Fleury briefly discussed the development of Mg components for aircraft in 1924. In the same way, there is a reference to the importance of hot briquettes, and the authors suggest that magnesium allocations can become easier, perhaps better than high-power AZ31. Still, the degree of deformation is critical for mechanical characteristics. Hutton described the use of an isothermal forging technique in 1939. Later, they reported higher formability in dropping stocks but better mechanical characteristics of the resulting forgings during low-temperature forging stages [27]. AZ31 has the following chemical composition: Mg - 2.9% Al - 0.75% Zn - 0.33% Mn - 0.03% Si wt% [28].

A wide range of magnesium alloy components is utilized in the aerospace sector, from gearbox and engine components to moldings for gearboxes, wings, fuselage leather, doors, buckets, seat components, and dashboard panels. Boeing 727 serves as an example because it has about 1,200 magnesium parts. Fig. 2.3 shows magnesium alloy usage in the aerospace sector. Mg is now used to create more vehicle parts than ever before [29].



Figure 2.3. Examples of magnesium alloy usage in Boeing 747: seat and wing components [29].

Because of its corrosion performance, its resistance is comparable to advanced and latest magnesium alloys. Similarly, the researchers showed interest in mechanical improvement and better corrosion resistance. Experts of the aerospace industry required sophisticated and more efficient magnesium compounds. Magnesium alloys work well in other applications, such as lightweight engineering applications, in which such alloys have significant advantages. In minimal-volume applications, manufacturers use zirconium-aluminium magnesium alloys. They perform casting, extrusion, and forging on them. The primary production of magnesium has increased because of the popularity of this metal and its alloys [23].

2.4. MECHANICAL PROPERTIES

Because of their chemical compositions, Mg AZ31 alloys have significantly different mechanical properties. Table 2.2 shows the basic mechanical properties of Mg and AZ31. This table was presented in a study conducted by Sunil et al., in which they examined the Mg alloy's properties, and they found that AZ31 was the only one that was within the 70-95 Hz range. Compared with other fragments of $\alpha + \beta$ phases, which were within the 36–48 μ m range, the indent length was 33 μ m in the β -phase dominated region [23].

Table 2.2. Elements of AZ31 [23].

Elements (wt %)								
Material	Al	Zn	Mn	Si	Cu	Ni	Fe	Mg
AZ31	3.05	0.82	0.40	0.020	0.003	0.0012	0.0023	Bal

At present, castings, in particular, are the majority of magnesium alloy commodities. Still, the microstructure of these products is not flawless and has poor mechanical qualities, which significantly impairs the broader uses of magnesium alloys. In the same way, the magnesium alloy deformation caused by plastic processing generally shows greater hardness and strength, so many structural components are required. Futuristic extrusion in wrought magnesium alloy manufacturing is widely-utilized for plastics. During the extrusion process, the material undergoes high hydrostatic

pressure, so massive deformations occur, which are beneficial for removing the acceptable structural defects in the alloy to be cleared and effectively enhancing the overall material properties. Forging and rolling are the main benefits of the extrusion process compared to other plastic processing methods. Extrusion technology is flexible and incredibly easy to use. Secondly, their accuracy concerning extruded products' surface quality and sizes is good. Extensive research analyzed extruded magnesium alloys. Cumulative extrusion occurred at 200°C at a 6mm/sec extrusion rate, and the extrusion ratio is 12.8:1 in the case of AZ31 magnesium alloy sheets with 1.4µm refined grains [30].

2.5. FORMABILITY OF MAGNESIUM ALLOYS

Magnesium has poor formability at average temperatures because of its hexagonal-shaped and envelope-like structure [26]. A research group has studied magnesium alloy sheet forming processes during recent years [4,26,27]. They observed that magnesium alloys' mechanical characteristics improve at higher temperatures [32] [31]. Considering Mg production through direct chilling or twin casting, some popular procedures help identify optimum processing parameters and explore new forming techniques [29].

2.5.1. Formability of AZ31 MG Alloy Sheets

Currently, magnesium alloy products undergo the die-casting process. On the other hand, traditional cast magnesium alloy cannot meet the growing industrial needs because of various casting deficiencies and low mechanical qualities of cast materials. In the same way, the magnesium forged alloys developed from plastic processing techniques, for instance, rolling, extrusion, and forging, which have garnered considerable attention because they improve the mechanical qualities of Mg and its alloys. Thus, the sheet forming procedure may be made viable as an alternative method that utilizes wrought magnesium alloys and ensures improved yields and final strength. Magnesium alloy forming technologies have become a significant development trend [32].

Mg alloys are interesting for researchers because they are the lightest construction alloys. Their expensive treatments at high temperatures (300-450°C), the magnesium alloys' low ductility restrict their applicability. Studies are necessary for promoting their industrial usage because of improvement in their properties at low temperatures, specifically at low re-crystallization temperatures. Magnesium alloys help manufacture bars, sheets, tubes, or wires through extrusion, rolling, and drawing. The appearance of the necessary roughness leads to the polar deformation process that greatly affects the alloy's properties. In the case of single crystals, $\langle 11-20 \rangle \{0001\}$ slips, $\langle 11-20 \rangle \{10.10\}$ and $\langle 11-20 \rangle \{10.10\} \langle a \rangle \langle a \rangle$ slips are known as magnesium slips while $\{10-11\}$, $\{11-21\}$, $\{10-12\}$, and $\{11-22\}$ are similar to the trend $\langle 11-23 \rangle$ but for many slips, the critical shear stress (CRSS) is quite diverse [34].

The researchers conducted the formability investigation of 1.2mm thick AZ31 sheets at high temperatures in various tests. Fuh-Kuo Chen and Tyng-Bin Huang conducted a study to investigate the mechanical properties of rectangular AZ31 samples at different temperatures from room temperature to 400°C. The researchers built a heating furnace for MTS810 test equipment and conducted high-temperature tensile tests. Experimental results indicated that AZ31 sheets' formability was poor at room temperature but significantly improved with the increased chance of local deformation, as shown in Fig. 2.4. They were "FEMed" more before breaking for shaping at a high temperature. In addition, testing is a part of the present study, which showed a conical cup value (CCV) of an ideal forming temperature of under 400°C. A low forming temperature requires an actual forming process [5].

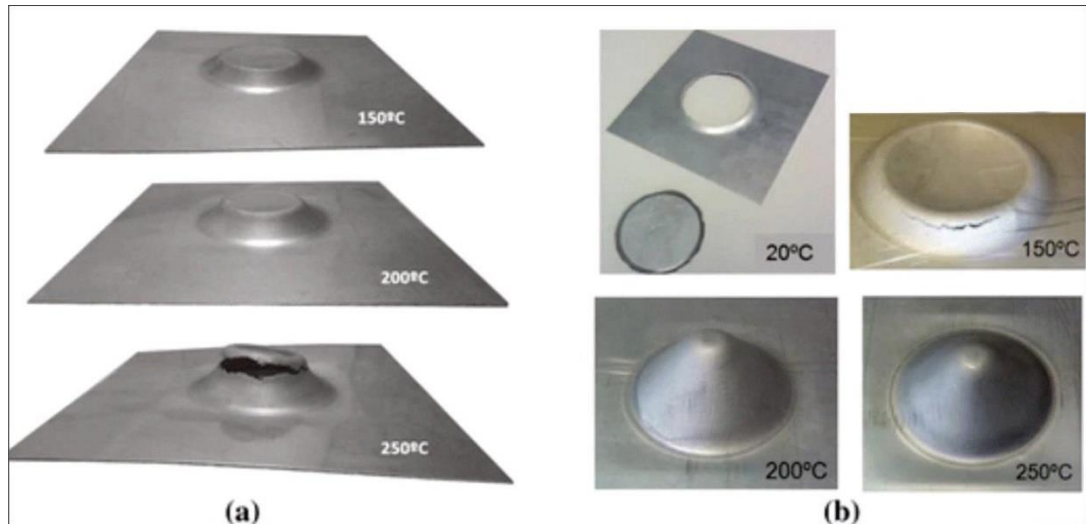


Figure 2.4. Broken magnesium conical cups were obtained from various experiments [35].

They selected additional parameters for simulation to examine the impact of process parameters, such as forming temperature and punch and die corner radii, on the AZ31 square cup formability. For example, 0.6mm die clearance on each side, 2.5KN blank holding force, 0.1 friction coefficient, and 3mm/s punching speed. The square cups of AZ31 sheets went through deep drawing at high temperatures to conduct the FEM analysis. The AZ31 sheets were poorly-formed if produced at ambient temperature, evident from tensile and shaping limit tests. The formability significantly increased when we stamped the AZ31 sheets at a high temperature. For both simulations and experiments with finite element analysis, the die radius (R_d) was 6mm, and boiler radius (R_P) was 5 mm, used to obtain the results. For drawing squares, 0.5mm thick laminates of AZ31 showed 2000°C as the optimum forming temperature.

In the same way, the thickness and shape of the pieces to be machined may differ from the ideal temperature. The simulation results show that a significant boiler radius results in a homogeneous substance, which flows in both directions. Delayed incidents occurred because of the cardinal rule under the eyelid profile at the corners. This pressure pattern shows why a large boxing radius helped increase the cups' formidability. Both thickness and shape of the pieces to be machined may vary from the ideal temperature. The finite element simulation results showed that the greater boiler radius permitted homogeneous material flow in both directions, in the cardinal

order, and below the eyelid profile at the corners that delayed incidents. This pattern of stresses explains why a bigger boxing radius helps improve the drawing cups' formability. The experimental data showed high consistency with the simulation findings for AZ31 plates and established the importance of square-cup drawing, optimum-shape temperature, hole-radius, and mold-angle radius [6].

2.5.2. Shearing Process for AZ31 Magnesium Alloy

There may be a fracture process, and this fracture may be brittle for the magnesium plate when the shearing force of the shearing machine is utilized for the sheets to cut them at room temperature [36] immediately. In the same way, the punching tool initially comes in contact with the metal plate during a typical shearing process, as given in Fig. 2.5. The punching movement then pressures the metal plate, passing the substance into the matrix. Compressive tension results in elastic sheet deformation, and the compressive tension goes beyond the work piece's performance strength, causing the plastic to FEM the sheet metal. Consequently, we adjusted the edges, as well as the cutting surface. At the margin of the perforated matrix, fracture begins to form. Finally, the elastic stress is released, creating adjustable vibration in the piece following separation from the perforated area [37].

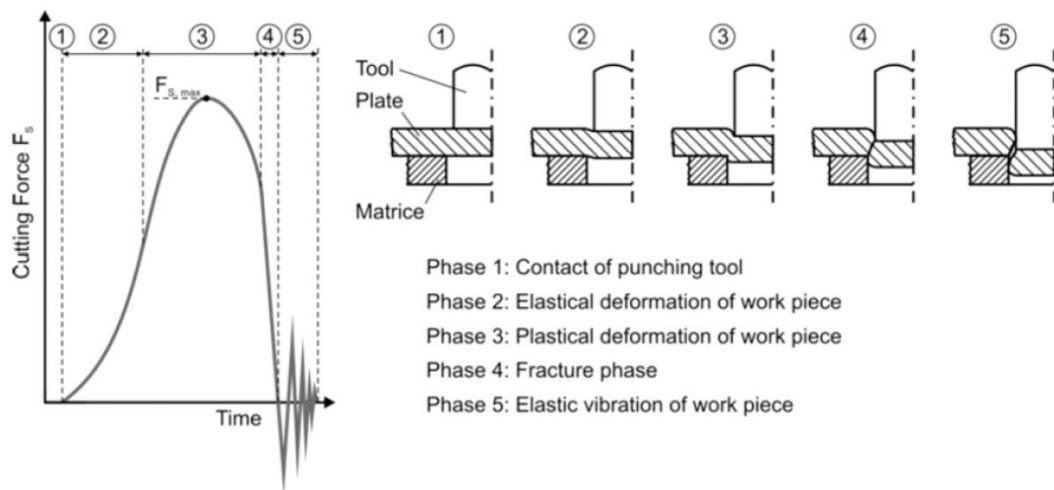


Figure 2.5. Conventional shearing process phases [37].

In the sheared formations, several secondary slit faults also occur. The crystal structure of the magnesium alloy plate does not easily deform. The fracture phenomenon quickly initiates after exerting large-format shear stress. In addition, poor deformation of the fracture during the shear fracture process may cause significant secondary damage. That can generate many deficiencies in the sheet shear properties, but after heating the alloy plate and before cutting, the quality of the shear sections significantly improves. Shear profiles, so optimized, can be easily achieved when the temperature rises.

In the same way, the highest quality of the sheared profile is 160-260°C because the cutting profile has no fracture defects at low temperatures. The worst deformation occurs in magnesium alloys, and Inter-crystallite fracture is complex, the primary cause of brittle cleavage division. The internal viscosity of the shear coil increases when the temperature is high, and its characteristics are poor; therefore, when the temperature is 160-260°C, it is better to obtain the sheared profile quality [36]. Fig. 2.6 displays shear deformation profiles and magnesium alloy damage at 100, 200, 300, and 400°C.

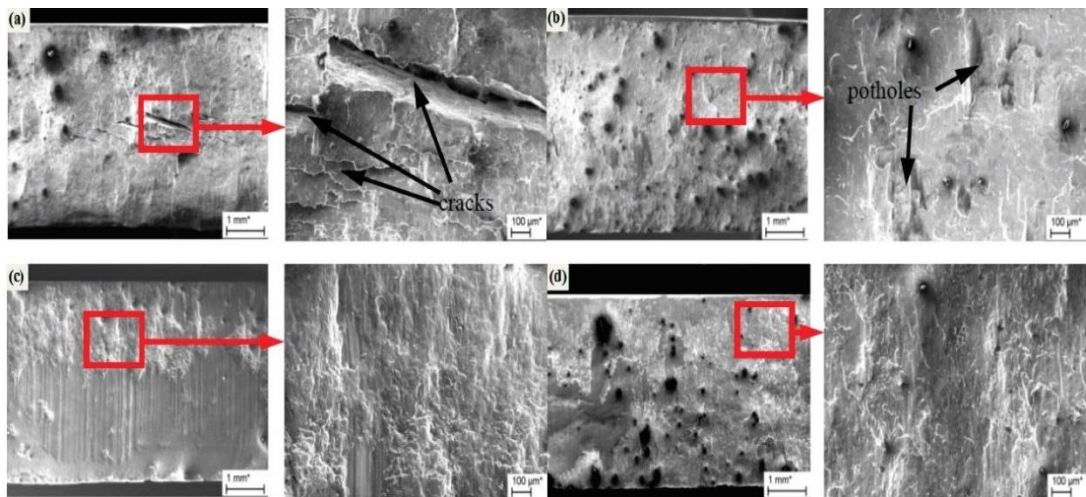


Figure 2.6. Comparison of typical sheared edge profiles at various AZ31 magnesium alloy temperatures: (a) 100°C (b) 200°C, (c) 300°C and (d) 400°C [36].

2.6. MAGNESIUM APPLICATIONS

Currently, magnesium alloys are light substitutes for steel and aluminium structural materials. In the same way, they gained great importance because they offer many advantages, including environmental friendliness, higher vibration absorption, high strength ratio, and light weight because of new forming techniques. This type of alloy shows the possibility of forming under lower temperatures. Moreover, these alloys enhance the heat resistance, and their strength extends for different applications [38,39].

2.6.1. Magnesium Application in Aerospace Industries

In the aerospace industry, magnesium alloys offer various advantages, but weight reduction is their main advantage. Magnesium is the lightest structural metal; it helps manufacture many aircraft parts. For example, ZE41 is a magnesium alloy for applications, which operate at up to 1500C because of its excellent mechanical properties. WE43 is another magnesium alloy that shows impressive strength and corrosion performance, and it is for new helicopter bodies, including Eurocopter EC120, NH90, Sikorsky S92, and MD500. Similarly, the aircraft manufactured using the same alloy can have a longer life cycle and have fewer overhaul requirements.

Another advantage of WE43 over WE41 is the fuel economy. In addition, magnesium alloys equally serve industries of military and civilian aircraft. This aspect includes various examples; for instance, Rolls-Royce Company manufactured the RB21 gearbox using EZ33 and ZE41, which help produce Tay engines. Many military aircraft, including Eurofighter Typhoon, F16, and Tornado, were manufactured using many magnesium alloying elements because of their lightweight features. Moreover, the manufacturing gearboxes of Pratt and Whitney F119 and American F22 aircraft use WE43 magnesium alloy because of their exceptional strength [39].

2.7. ADVANTAGES AND DISADVANTAGES OF AZ31

This section includes the advantages and disadvantages of magnesium alloys over traditional ones such as natural fiber, titanium, Mag alloy AZ31, steel, and polymers.

2.7.1. Advantages of AZ31

The advantages can be summarized as follows [40]

- Low-density that makes metallic materials suitable for all the construction uses
- Provides maximum acceleration due to low density
- High strength-to-weight ratio
- High strength
- Good machinability, castability, and easy availability
- Suitable for high-pressure die-casting
- Possibility to mill and turn in a controlled atmosphere
- Weld-ability in a controlled environment
- Enhanced corrosion resistance.
- Compared with polymers, magnesium alloys have better aging resistance, mechanical properties, better thermal and electrical conductivities, and are recyclable.
- AZ31 category has low latent heat, providing better dimensionality, smaller curved surface, surface quality, better draft angle, and more specific strength (14% more than aluminium).

2.7.2. Disadvantages of AZ31

Despite the advantages of magnesium alloy mentioned above, it has many disadvantages, which can be summarized as follows [40]:

- Limited cold workability and toughness
- Low elastic modulus
- Limited creep resistance and strength at high temperatures

- High chemical reactivity
- High shrinkage after solidification
- Little corrosion resistance in some applications
- Limited applications because of low strength, poor elasticity, and poor cold workability

2.8. EFFECTS OF SHEAR-DAMAGED AREA ON MAGNESIUM ALLOY AZ31

AZ31 sheets at average ambient temperature lead to an unusual zigzag fracture on the shear edge, hindering future forming processes [36]. The hexagonal packed crystal (hcp) structure of the AZ31 plates leads to pattern anisotropy at room temperature [41]. Limited plastic deformation occurs at ambient temperature [41]; however, non-basal deformation activates within the temperature range 150-250°C, and the material ductility significantly improves [42].

If we cut a magnesium alloy plate at room temperature, the cracks will spread once they move with the thickness of the material. Instability in crack growth can prevent more fractures from going down several paths, resulting in small cracks. In the same way, the random crack pattern affects the geometry of the shaved arcs, resulting in a wild type of fracture. The secondary curved fracture profile exists at 25°C and 100°C in the cutting arms through optical micrographs. Figures 2.7a and b show a scanning electron microscope image at 25°C.

Similarly, the removal of 20% micrographs at 100°C shows the same defects in the tensile curved fracture profile. Fig. 2.7a shows an odd coil fracture profile on a sheared edge, which results in early failures in the later forming steps. At 150°C cutting temperature, the clamping fracture and its shape remove. Figure 2.7b shows the SEM fracture profile image at 250°C, equivalent to 20% purification [42].

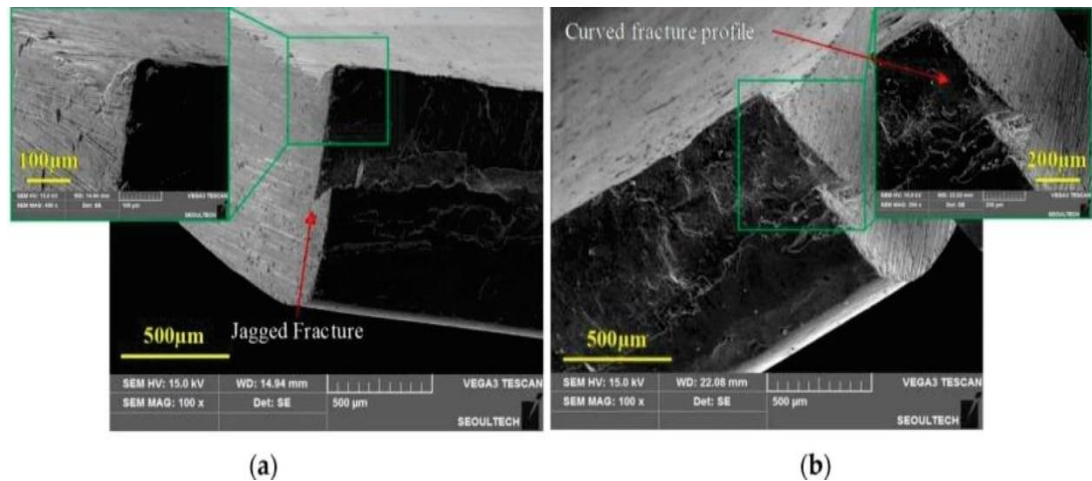


Figure 2.7. Fracture in magnesium AZ31 (a) A primary rough fracture is shown on the side; (b) The profile of the secondary curved fracture is shown on the side [42].

2.9. VARIOUS HOLE EXPANSION MAGNESIUM ALLOYS

The manufacturing of magnesium alloys produces just like other metals. Still, as far as magnesium alloys are concerned, they are difficult to manufacture at room temperature, so most procedures occur at high temperatures. In the same way, it is essential to heat the metal, use a die, or both. Shears with blades, white die cutters, routers, or saws can be cut from magnesium alloy sheets and usually utilized for cutting extrusion into long or circular cuts. Conventional cuts do not work well for magnesium alloy plates because the cutting edge is sharp and rigid, and the shearing and slicing of magnesium sheets is uneven. Maximum clearance exists within 3-5% of the sheet thickness. The top scissor blade needs a ground angle from 45° to 60°. The hole-cutting should be from 2°-3°, and the die angle should be 1°. The cutting tip of the die should be 2 to 3 degrees with a 1-degree angle to free up the drill bit for cutting. This procedure involves removing the second mowing of around 1 to 32 inches [43].

Sometimes hot shearing is utilized to assure a better edge. For heavy sheet and platform stock, this is necessary. The sheet can heat to 600°F, but the sheet with hard rolls should be below 400°F, depending on the alloy utilized after cooling. The thermal expansion requires shrinkage. Sawing is the only method to cut boards more than ½-inch thick.

In the same way, a circular saw helps cut small/medium extrusions with six teeth per inch. A researcher should use bucket-tooth or straight-toothed saws with eight teeth per inch to cut the sheet stock. Band saws should have non-stop blade guides to eliminate sparks, igniting the magnesium alloy filings. Cold working magnesium alloys are quite restrictive at room temperature because they are quick and do not go through extreme cold forming. Minor bending is possible to occur in the sheet material. Alternatively, the bending radius should be at least seven times compared to the soft-material thickness and 12 times the hard-material thickness. For the forming process, if a material is heated, the radius should be 2 or 3 times the thickness of the board [43].

2.10. ANGULAR STRETCH BEND MG AZ31

Both bending radius and temperature affect the reaction surface. In particular, only if operated at the lowest temperature the response surface will be the way, as Fig. 2.8 shows. The change takes place along the BEND-RAD axis. At 80°C, the stretching strength improves (using an 8mm die, the maximum load is more than the material at 80°C, and the die has a 2mm radius). This behavior does not change when the radius rises at 240°C [44].

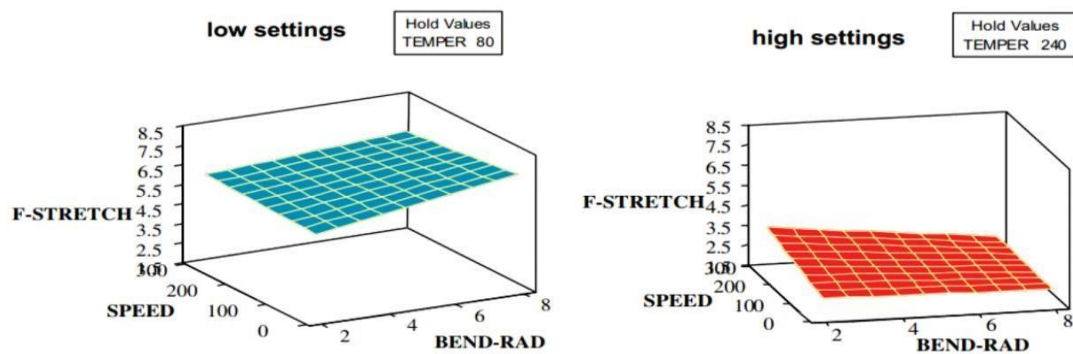


Figure 2.8. The average value influences the highest degree of stress and the bending radius (STRETCH) [44].

The creation of lightweight parts is one of the main priorities of many industries nowadays. Since magnesium (Mg) alloys have a very low density, more attention has been paid to them during the past two years, especially in automotive applications [44]. It is possible to use the fuel economy of automobile transportation by using specific

materials which have a favorable strength-weight ratio, for example, magnesium [45]. Inactive deformation mechanisms are essential at room temperature for improving ductility and magnesium alloy formation [45,46]. Unlike traditional stress test data, tensile stress and transverse bending (scanning) happen during sealing (for example, in packing radius regions). Both numerical and analytical models have been proposed in this context to predict the tensile and flexural strengths of AZ31 alloy either in warm conditions or at room temperature. The sidewall thickness of the undiluted punch-hole region decreases [45]. The research focuses on stretching magnesium alloy microplate stress and bending state in hot locations based on the test data.

PART 3

SHEET METAL FORMATION

This part of our study includes a detailed review of the punching process describing blanking, punching, and piercing. Also, it contains several details about the sheet metal punching process, punching operation, clearance of die, and hydraulic punch process. In the last section of this part, we have provided excerpts from many previous studies about the punching operations using AZ31 alloy.

3.1. PUNCHING (PIERCING AND BLANKING)

To modify the existing blank, punching, blanking, and piercing are sheet metal shearing operations. Besides, various punch, die, and similar machines also help perform the mentioned operations. Piercing and blanking involve a punch and a die used for manufacturing parts using either sheet stock or coil. Blanking produces exterior features of a component, but piercing makes internal holes/shapes. After the production of multiple pieces, the web came into existence. Then, the obtained parts were scrap materials. Moreover, "slugs" produced through piercing interior features were also considered scrap. It is possible to use "piercing" and "punching" interchangeably.

While punching, the punch removes some materials from a large piece or a sheet metal strip. In the case of discarding the small part, it is punching, but the remaining portion is scrap if the small removed piece is required. In that case, the operation is called blanking [47]. The following descriptions show blanking, piercing, and punching [47]:

- **Blanking:** Figure 3.1 shows this process. Blanking is a process used to cut sheet metal, utilized to manufacture an enclosed-sheet metal part out of a large sheet metal piece by applying high shear force. The blank part is the finished product

In most cases, blanking is a metal sheet cutting process through which the desired flat sheet of an end part is cut [47].

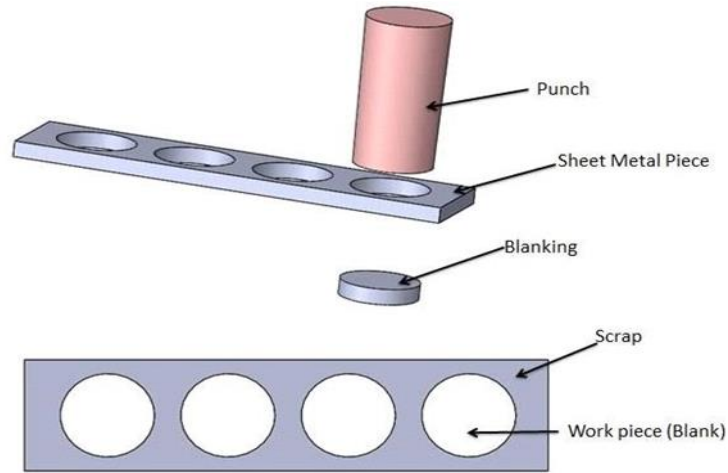


Figure 3.1. Blanking operation in sheet metal [47].

- **Punching:** Punching is another metal sheet cutting process involving removing scrap material from large chunks of metal sheet using a high shearing force. Similarly, the punching operations combine in different shapes (mostly rectangular and circular) and sizes for manufacturing finished sheet metal parts, as Figure 3.2 shows.

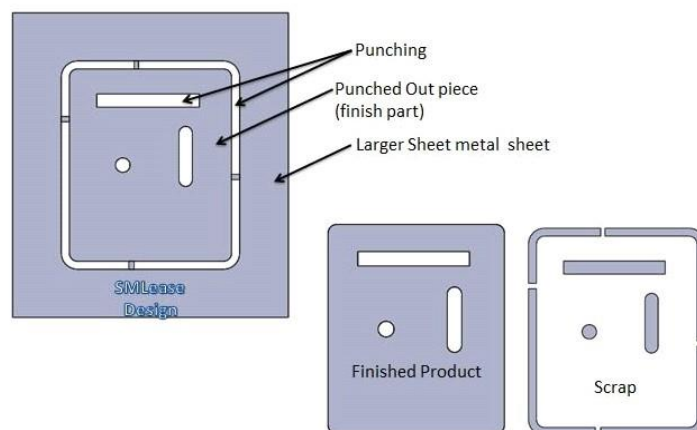


Figure 3.2. Punching operation in sheet metal [47].

- **Piercing:** Piercing creates an extruded hole or slot in a metal sheet in sheet metal punching operation. Moreover, the piercing procedure combines forming and cutting processes.

3.1.1. Sheet Metal Punching Process

It is one of the most popular manufacturing and industrial processes. Conventional punching processes have many failures, including tool misalignment, broken tools, tool wear, and slug jamming [48]. These failures may interrupt the production process or deteriorate the quality of the hole. In the same way, it is necessary to monitor the punching process online and timely detect and correct the punching failures, which helps confirm the product quality and protects the tools from different types of damage. Since sheet metal processing is a quick process, it processes the sheets in a dozen milliseconds or less. The data collection method and the feature extraction process, which characterizes the punching procedure, are significant to conduct correct operations [48].

3.1.2. Punching Operation

Whenever the punch enters the punching die, the punching operation removes the scrap slug from the metal workpiece [48]. A hole remains in the metal work piece because of this process. Sectional dimensions help determine the shape and size of the created hole in the work piece [48]. The slug falls through the die from the hole to a specific container for disposal or recycling. The upward movement of the punch pulls the sheet along, and the sheet releases through a stripper. The rim quality improves if the cut friction on the sheet edge increases. Suppose a punch wears, the slug frequency or the frequency of putting the sheet increases, which worsens the hole quality.

In the same way, the blanking process looks like the punching process, which removes the metal workpiece from the metal strip/sheet when punched [49]. The removed material is either the new workpiece or blank. From the metal forming standpoint, punching and blanking are the same, as presented in Fig. 3.3. The processing and tooling are the same for both operations, but the punching process is the only

difference. In punching, the punched-out piece is slug or scrap, while the punched-out part is helpful in blanking. The punching operation causes a sudden change in the pressing force because of the transient nature of the material, which can break when shear strength is applied. Fig. 3.3 shows the typical force-time curve in the sheet-metal blanking procedure [48].

A sudden drop occurs whenever scrap removes from the sheet, and vibration decay occurs. The force characteristic is in the sheet metal blanking and punching process [48]. The punching scrap is mostly smaller than the blanking product, so there is an extended metal forming period in the blanking process compared to punching. The force curve change refers to the difference in the process, but punching causes vibration decay. It includes the information regarding the process change [50].

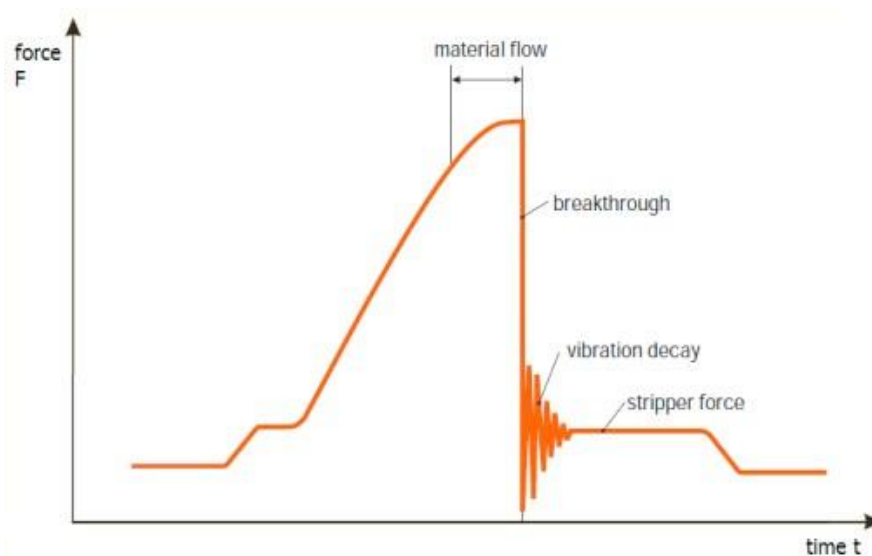


Figure 3.3. The force-time curve for sheet metal blanking and punching [48].

3.1.3. Die Clearance

The punch-die distance represents the die clearance, as Figure 3.4 shows. The edge is commonly included in four sections, as shown in Figure 3.5. Compared with blanking and punching in mild steel, the selection of die clearance more significantly affects the tool life; therefore, the burr formation is small and not highly influenced by changing the die clearance: the fracture area and rollover increase [51].

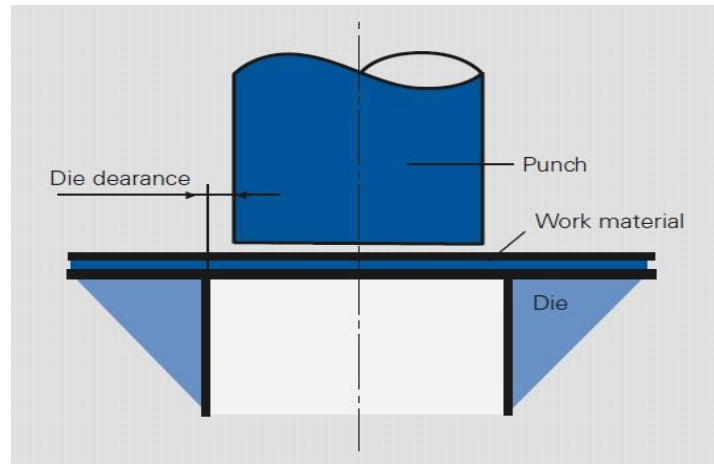


Figure 3.4. Die clearance definition [51].

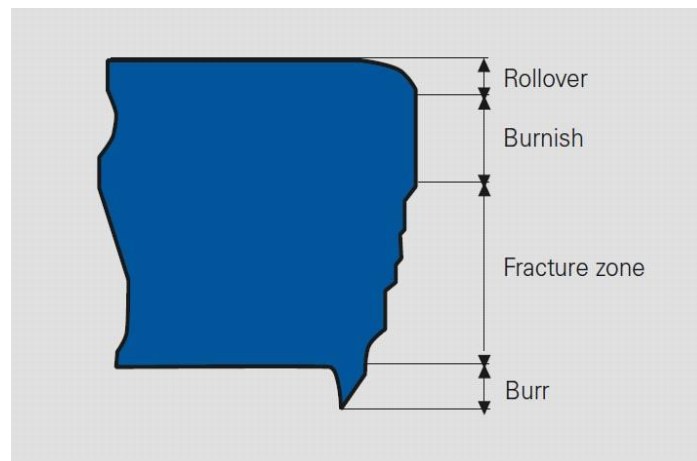


Figure 3.5. The appearance of a cut edge [51].

3.1.4. Hydraulic Punch Press

A hydraulic punch process powers ram using a hydraulic cylinder instead of the flywheel, and it is controlled either through a feedback mechanism or a valve [50]. A valve-controlled machine generally allows a single-stroke process, enabling the ram to stroke up and down when ordered. In the same way, the controlled feedback system allows the ram to be regularly controlled through fixed points when requested, as displayed in Figures 3.6 and 3.7. It permits a more considerable control through the ram stroke and increases the punching ratios when the ram does not have to complete the traditional full stroke of up and down movements. It can work inside a concise stroke window [50].



Figure 3 6. Hydraulic punch press.

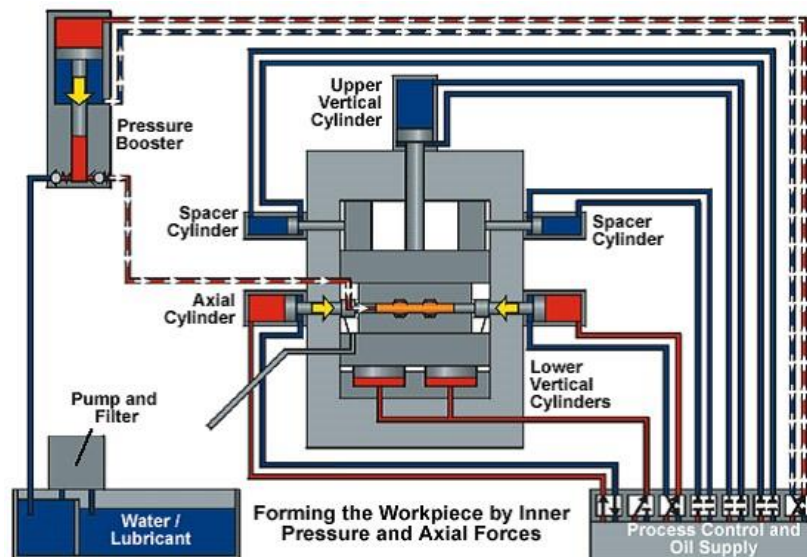


Figure 3.7. The layout of the hydraulic punch press [50].

3.2. RELATED STUDIES

So far, many researchers have investigated the punching process. In this section, we will provide some studies on the punching process of magnesium AZ31 with diverse punching tips, which are as follows:

Grigoras et al. [52] conducted an experimental study by analyzing the AZ31B magnesium alloy sheet failure through punch stretching. In the same way, the researchers found that the magnesium alloy sheet formability at room temperature

results in variations in the mechanical difficulties and properties, specifically in terms of cracks in zones with bend radius. Moreover, the elastic spring back is essential, which leads to massive deviations in the required shape [52]. The study is on magnesium alloy AZ31B sheet with 1mm thickness and its formability when stretched at room temperature applying many dies with various radii. The stretching process was performed on the hydraulic press using the following 3D printed PLA: R180, R320, R540, R720, R900, and R1080. The stretching of samples was continued until the fracture occurred, which involved variables such as distance to fracture, fracture force, bend angle, and deviation from the die radius.

Fazily, Yu, and Lee [53] conducted an analytical study to analyze the finite elements of the AZ31 sheet's blanking operation applying the ductile fracture criteria and its verification at different temperatures. A computational analysis compares the obtained experimental results. The blanked edge shape and fracture initiation were affected when the finite element model used the critical damage criteria value. We calculated the essential criteria value and compared the ductile fracture criteria that many researchers have proposed so far using different process parameters and temperatures. Another study was conducted to investigate the effect of temperature and other process parameters on blanked-edge geometry, for instance, burrs, rollover, fracture area, and shear surface.

Xue, Yan & Kang [54] numerically studied the AZ31 and 7050 Mg alloys' limit diagrams to test the mentioned alloys' formability levels. At room temperature and in warm working conditions, the formation of limit diagrams for AZ31 magnesium alloys happened by extracting the in-plane strain of the surrounding elements. They obtained the strain values of the most significant strain element when unstable. The Nakazima presented the virtual model in the study, which shows that it can accurately predict FLD. Moreover, the study investigated the effects of virtual punching speed and lubrication on the AZ31 and A7050 bulging processes. The results show that sheet formability will be better when the punching speed is lower, or the lubrication environment is good. Punching speed reduction significantly affects the AZ31 sheets' formability.

Palaniswamy et al. [55] studied a magnesium alloy sheet formed at a high temperature using FEM. The study outcomes indicate that the punch temperature plays a significant role during the warm forming process. It also affects the temperature of cup walls and increases their strengths compared to the flange. Moreover, the comparative analysis of the same study shows the simulation results over the rate at each temperature.

In an experimental study, Chang et al. [56] studied a warm deep-drawing sheet of AZ31 magnesium alloy. AZ31 magnesium alloy sheet fabrication shows excellent performance through uniform annealing and cross-rolling procedures. They used Gleeble 3500 thermal-mechanical simulator to conduct uniaxial tensile experiments and analyzed the AZ31 magnesium alloy's mechanical properties. In the end, they also conducted some Limiting Drawing Ratio (LDR) experiments. The results indicate that LDR could access 2.0 at 150°C, forming temperature and 15mm/s drawing speed. Then, we simulated the warm drawing process using the finite element approach. The study also includes a numerical investigation of formidability, drawing temperature, and blank holder force. The simulation shows that the variable blank holder force technology can enhance the LDR from 3.0 to 3.5 and reduce the wall-thinning rate from 15.21% to 12.35%.

Liu, Liu, and Wang [57] conducted another simulation study to understand the AZ31 sheet rolling process and the difference between 2D and 3D simulations. For the mentioned analysis, 2D and 3D FEM results showed good agreement with the experimental results, but this depends on selecting the correct parameters of the AZ31 stress-strain relationship, the coefficient of interfacial heat transfer, and the friction element with/without lubricant. The study has also illustrated the effects of rolling, roller temperature, and workpiece temperature on the rolling torque/load and the difference between the simulation results.

PART 4

EXPERIMENTAL AND THEORETICAL ANALYSIS

This study used Mg AZ31 alloy at different strength levels and three geometries for the punching operation. First, we examined and obtained three Mg AZ31 samples using digital microscopy and SEM technology, and we compared them to experimental studies' results. Additionally, we considered shear surfaces and fragments as well. The flow chart given in Figure 4.1 shows the stages and methodologies of the study.

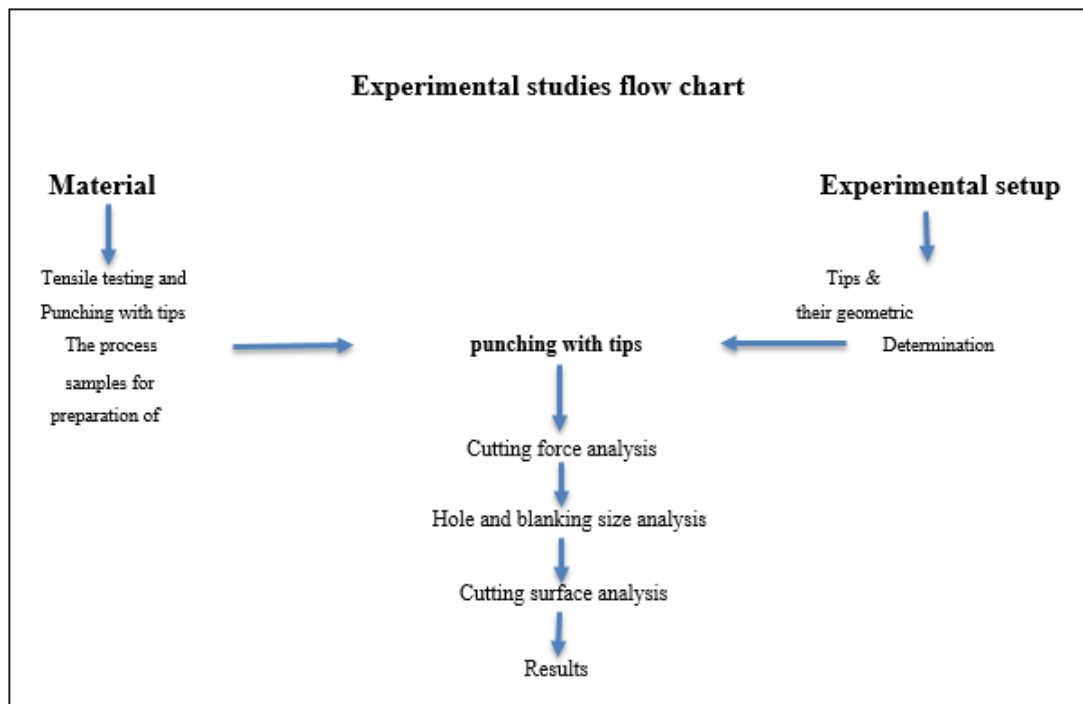


Figure 4.1. Experimental flow chart.

4.1. MATERIALS

This research study used the commercial alloy Mg AZ31 in hot-rolled condition with 3mm sheet thickness. Moreover, we cut the punch samples into small strip pieces of 151x27mm each for the study. We purchased the sheet materials. Table 4.1 shows the AZ31 alloy's chemical composition Fig. 4.2 shows its microstructure.

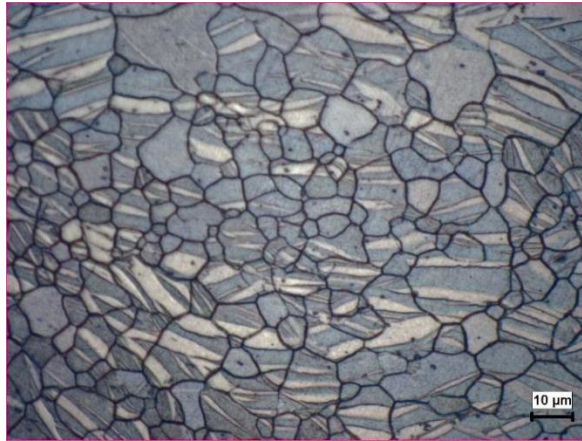


Figure 4.2. Microstructure of the used AZ31 alloy.

Table 4.1. Chemical composition of the used AZ31 Mg alloys.

Elements	Al	Zn	Mn	Cu	Mg
% Weight	2.83	0.80	0.37	0.002	Rest of

4.2. TENSILE TEST

We used Zwick/Roell 600 KN machine to conduct the tensile tests according to ISO 6892-1 Standard and 2mm/minute tensile velocity. Figure 4.3 presents the tensile test sample:



Figure 4.3. Tensile test samples of Mg AZ31 alloy.

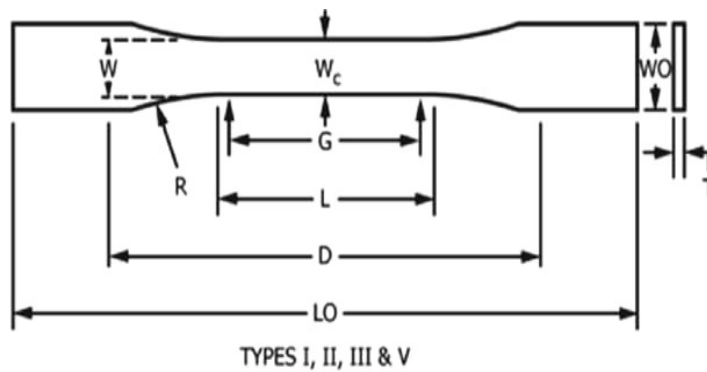


Figure 4.4. Dimensions of standard tensile test samples.

We cut the tensile test specimen using a water jet according to specific measurements, including the overall length, the distance between shoulders, gauge length, grip-section width, grip-section length, and width of the reduced specimen, which is proportional to gauge length L_0 . L_0 has a relation with the original cross-sectional area A_0 , and this relation is $L_0 = k\sqrt{A_0}$. In EN specifications, the constant k is 35. It helps determine the overall specimen diameter and, obviously, 4 x specimen diameter. Despite the lack of significance of a few parameters, it is essential to find them to comply with specifications.

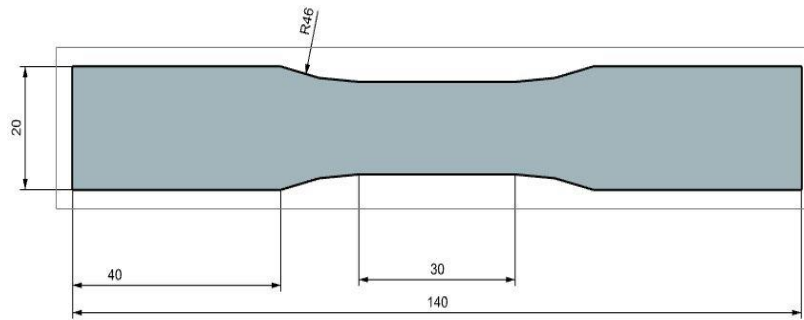


Figure 4.5. Dimensions of Mg AZ31 alloy samples for tensile test.

Figure 4.4 and Figure 4.5 show the dimensions of the tensile test specimen. We used a tensile testing machine for most basic and standard mechanical tests [58]. After applying tensile stress to a material during the tensile test, we measured the specimen response [59,60]. For this study, we conducted a tensile test of Mg AZ31 alloy.

4.3. PUNCH GEOMETRIES AND PUNCHING PROCESS

Among the metal forming operations, the punching process is a widespread technique. This process involves cutting a metal sheet/plate in a circular profile using a shearing mechanism [61]. We used a pair of sharp edges for the shearing action with the help of a die and a punch. It is economical, simple, and fast for the production of high-volume parts as compared to fabrication processes, including drilling and casting [61]. Still, the punching process is prevalent in many sectors, such as the automotive, electrical, electronics, petrochemical, and aerospace industries [61-64]. Manufacturers consistently improve productivity because of the ever-increasing demand for high-quality and cheaper products. Increasing the punch and die life is an important parameter essential for the punching process [61-64].

The sheared surface increases due to reducing the punch force and improving the work hardening; so, developing a punching process is quite challenging. This type of challenge can resolve through the proper selection of punch geometry. Selecting the appropriate geometry is also a challenge because the studies on the effect of punch geometry on the punching process are rare. This study investigates the impact of the

sheared surface, work hardening, and punch force using commercially available Mg AZ31 sheets.

Manufacturers use the forming process for manufacturing sheet metal components, like electronics, medical equipment, or automobiles [65-67]. Various experiments and analyses have been carried out in the drawing process by Colgan and Monaghan [68] and Yoshihara et al. They analyzed the blank-holder force control on magnesium alloys [69]. In a study, Aminzahed et al. investigated the effects of holder size and pressure on a rectangular micro deep drawing [70]. In another study, Lou et al. analyzed the impact of surface roughness on the circular cups' micro deep picture [71]. In a later study, Behrens et al. analyzed the effect of tool geometry on the limiting drawing ratio [72].

A hydraulic punch press machine performs punching operations: punching blanking, piercing, and sheet metal punching. In the same way, a scrap slug is removed from the workpiece through the punching operation whenever the punch enters the punching die, and besides, the die clearing process was also used. The experimental setup was integrated with a computer to record force data during the punching process, Figure 4.6 and Figure 4.7 illustrate. Figure 4.8 shows that the force data received through the load cell with high power capacity were processed through the A/D converter and recorded with the help of computer software.

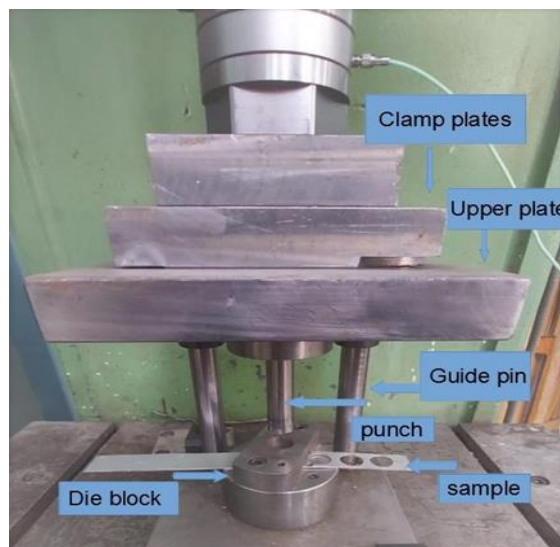


Figure 4.6. Experimental setup of punch-die with samples.

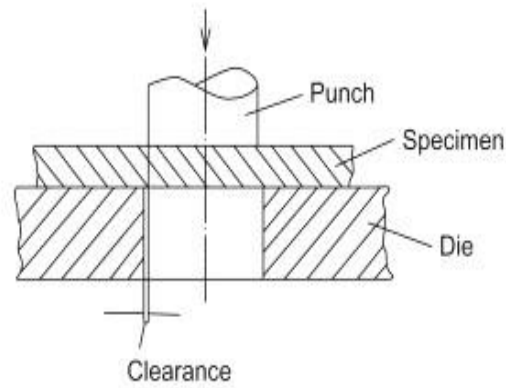


Figure 4.7. Schematic assembly of a punch test [73].

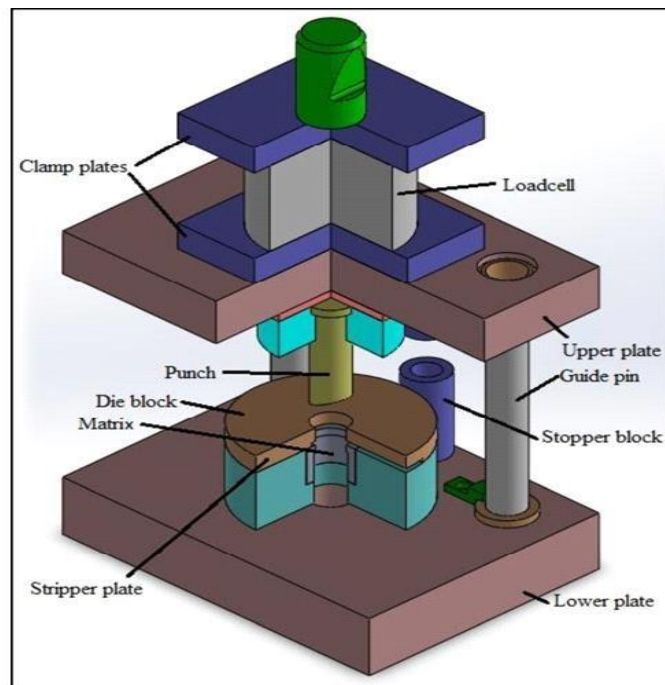


Figure 4.8. Schematic assembly of a punch test.

Bai and Dodd [73] mentioned that a punch test is simple while designing a flat projectile or punch. A simple punch test includes a schematic assembly to investigate the material propensity, which is needed to understand the adiabatic shear-failure behavior, as Fig. 4.8 depicts. The specimen loading can be done, for instance, by a modified Hopkinson bar [74]. A falling weight accelerated the punch (Fig. 4.8) and achieved up to 23m/s loading velocities. We have shown the performance of dynamic punch tests through a direct Hopkinson bar assembly in Fig. 4.8. We used three

different punch types for the punching process, and the distance (clearance) between the punch and die was kept constant. As mentioned before, there were three punches in the dynamic punch tests, so each sample had three punches, and we performed every test twice using the same force and speed. Then, we used the punch to induce stress concentration on the material, and adiabatic shearing started to form. The punch wholly penetrated the specimen plate. The recorded force-displacement behavior shows the material property. The punch-die distance and the die radius influence the results [64]. Because of the mentioned disadvantages, the punch test is not ideal for studying shear bending test samples of Mg AZ31 alloy.

For optimum punched hole quality, the punching process has undergone continuous development, which has made it possible to get the desired results with a low punch force. Furthermore, some parameters affect the punch force and punched holes, for example, material temperature, punch velocity, punch-die geometry, and punch wear. We used Mg AZ31 alloy and pure titanium to study the effect of the mentioned parameters [67,75]. Xu et al. declared in a couple of studies [67, 75] that punch velocity and clearance affect the brass sheared surface and surface roughness. They also found that punch velocity decreases the surface roughness and increases the burnish height, but burnish size reduces when clearance increases. A couple of studies show the use of the electro-pulsing method for investigating the impact of material temperature on the punch force, strength, and sheared surface [67,76].

4.4. PERFORMING PUNCHING PROCESSES WITH FINITE ELEMENT METHOD

Excessive deformation and strain formations make the punching process very complex to understand. This complex phenomenon has become relatively easy by using finite element modeling or FEM. FEM is now a popular process [77]. It is partly because of more freedom in terms of reinforcement distribution and geometry and mechanical properties of the interface because of computational power advances and user-friendly codes [77]. Elastic models, which contain thousands of elements, can be constructed and solved quickly using sophisticated computers. High-quality punching processes

with FEM provide an economical and fast solution. Under similar conditions, we conducted the SIMUFACT and finite element analysis.

Furthermore, correct material models helped obtain incredibly realistic data using drilling processes, which many research studies focused on gaining clearance, punch speed, punch strength, punch geometry, hole profiles, and force. This research study is about punching geometry, punch processing, punching blanking, and piercing. The sample sheet Mg AZ31 alloy has undergone punching process tests presented in Fig. 4.9. The punching operation removes the scrap slug from the AZ31 workpiece whenever the punch enters the punching die, and besides, we performed die clearance. Furthermore, FEM has been used to analyze the finite element method.



Figure 4.9. Mg AZ31 sample sheet.

Each test has been done twice within the same strength and constant speed conditions, as presented in Fig. 4.10 below, which shows the outcome of the punching process.



Figure 4.10. Experimental test based on punching processes P1, P2, and P3.

The application and subsequent modeling of punching processes with punching and modeling help in cost reduction, a comprehensive study, and experimental work. For

this reason, we used the Simufact program to conduct the tensile tests. Their results were compared using the experimental tensile test data. Verifying the material model is a significant factor in the precision a computer's punching process. Then, we performed three punching operations in 2D and 3D simulation under three boundary conditions, and we compared them with experimental data p1, p2, and p3. We conducted experiments using SIMUFACT and finite element analysis.

4.5. MEASUREMENT OF THE DIMENSIONS OF PUNCHED PARTS



Figure 4.11. Dimensions: Thickness 3mm, length 151.26mm, and width 27 mm.

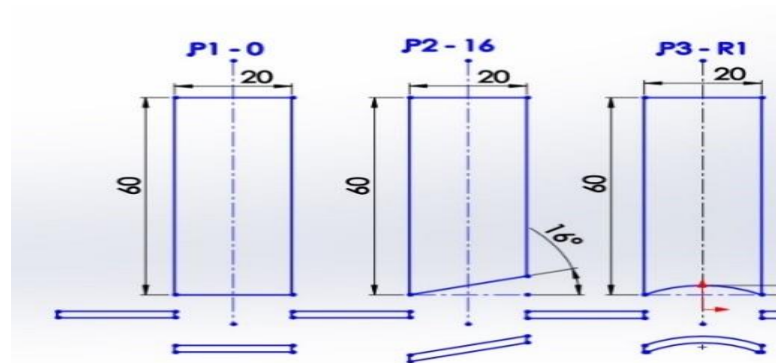


Figure 4.12. Dimensions for all punches P1, P2, and P3 (20mm).

4.5.1. Punched Part Images and Failure Analysis

We applied digital microscopy and scanning electron microscopy (SEM) for punch part images and failure analysis. The samples were divided into two using a saw for cutting surface analysis. An examination of the cutting surface resulting from the

punching process using 3 punching tips is shown in Figure 4.13. (a) flat P1 (0°), (b) concave P2 (R) and (c) angled P3 (16°) which were obtained from the literature [78].

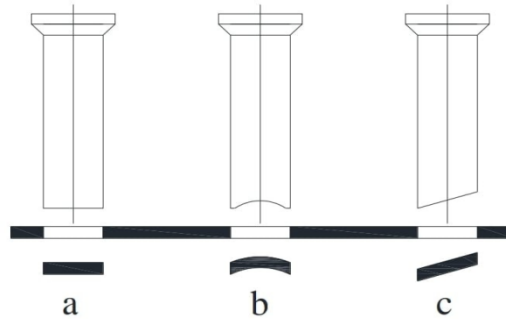


Figure 4.13. Punched and cut part [78].

We conducted a damage analysis investigation in the study, as shown in the flow chart in Figure 4.14.



Figure 4.14. Flowchart of damage analysis.

PART 5

RESULTS AND DISCUSSION

The punching process, extensively used in the manufacturing industry, involves punching a hole in the workpiece [78]. It is one of the most significant sheet metal manufacturing processes applied for the mass production of metal components [65]. Technological aspects of this process can be understood by understanding the functions of different punching tools. We separated blank metal from the sheet during manufacturing for the blanking process. For conducting the punching process, we made holes of various forms and sizes in a blank-sheet metal, for which we used a punch tool for separating a sheared piece from the sheet. Both processes (punching and blanking) are conducted [64]. Moreover, both the mentioned processes significantly influence different manufacturing industries, including the airplane industry.

Hydraulic, eccentric, and turret punch presses are the most common presses used with punch tools. For simulation, SIMUFACT and FEM are commonly used to analyze several heat treatments and forming processes, valid for AZ31. Both the mentioned forms of analysis help resolve non-linear and time-dependent problems and find solutions in discrete time increments. Variables, including speed, temperature, and others, are determined through both the processes based on time increment, but the answer also depends on boundary conditions.

5.1. TENSILE TEST

5.1.1. Tensile Test and Fracture Mode

Several investigations have been carried out on the Mg AZ31 sheets [4,10]. A study investigated micro-fracture using a commercially extruded AZ31 with 200 μ m grain

size. Three SEM magnifications of AZ31 were applied, including $2\mu\text{m}$, $20\mu\text{m}$, and $200\mu\text{m}$, as shown in Fig. 5.1A, B, and C. Fig. 5.1A shows the lower magnification image, in which a dark area appears that indicates the fracture surface. A high magnification image (Fig. 5.1B) shows a ductile fracture, which shows the separation of atoms. Other than the brittle fracture, ductile fracture microstructures appeared in the shape of microvoids [79]. Fig. 5.1C depicts how voids are formed and distributed. They are in the form of dimples on the fracture surface, called microvoids.

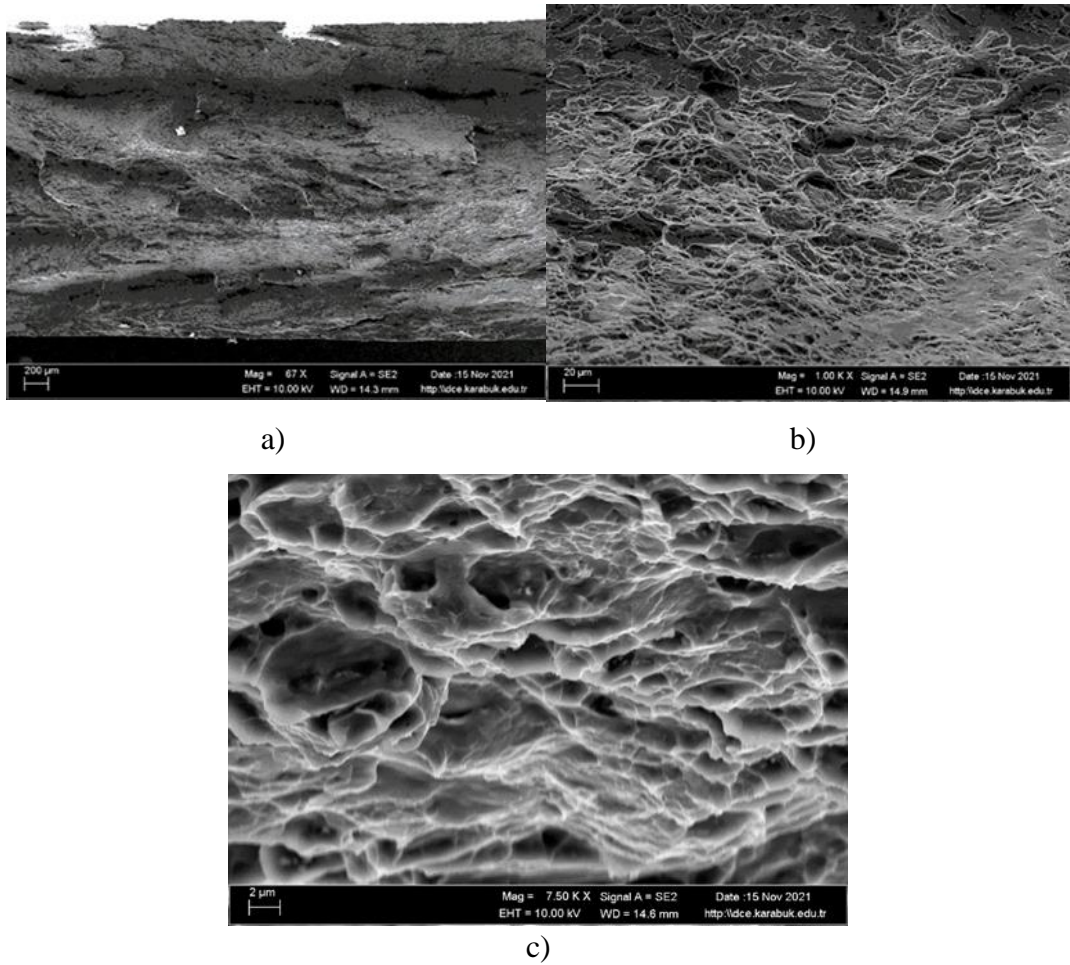


Figure 5.1. A-C. Mg AZ31 alloy microstructure.

We performed a tensile test to determine the Mg alloy's tensile strength [58]. This procedure includes a test specimen loaded in a machine. The machine grips on one end, and axial tensile force is applied [59]. Then, the device continuously and slowly stretches the test specimen at a specified and standardized rate and carries on until a failure occurs [60]. After imposing the stretch, we recorded the opposing force in the

test specimen and plotted it on a graph for the applied elongation: the fracture mode and the tensile test (Figure 5.2).

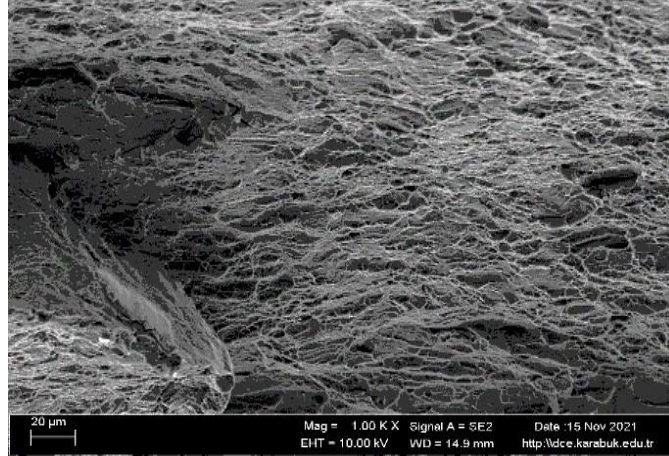


Figure 5.2. Tensile test and fracture mode.

Figure 5.2 indicates the fracture mode and the tensile test applying a commercially extruded AZ31 workpiece with 20 μ m grain size. The pictures show the entire fracture process, which took place in the region of the final rupture. Many simple patterns and fracture points appeared on the fracture surface, and we have shown fracture modification using the red line.

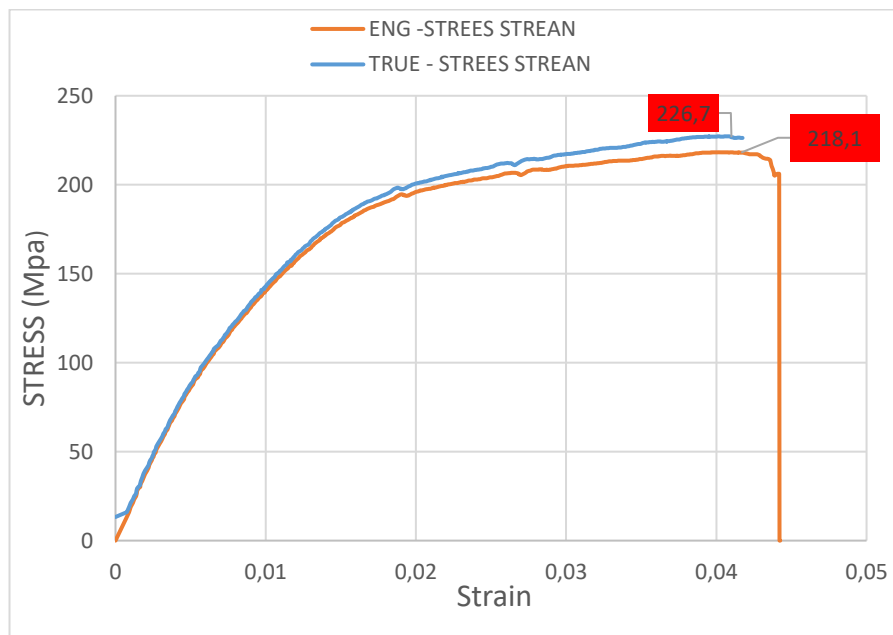


Figure 5.3. Engineering and true Stress-Strain Curve for Mg AZ31 alloy.

Figure 5.3 shows that as a consequence of performing the tensile test, yield point (YP) bore the strain and applied the stress below the yield point where the deformation changed the Mg AZ31 behavior. It means that the specimen returns to its actual length below the yield point, but permanent deformation occurs to the sample after the yield point. We observed two facts through the tensile test of Mg AZ31: Observable AZ31 deformation begins at 218.2149089 while the maximum load intensity, which can carry the tension, is below that point. The strain, the reduction in the cross-sectional area, and the Mg AZ31 alloy stretch all occurred because of stretching. It is possible to determine the AZ31 rupture/fracture point, and the red line shows fracture modification.

5.1.1.1. Tensile fracture mode



Figure 5.4. Tensile test measurement after the test.

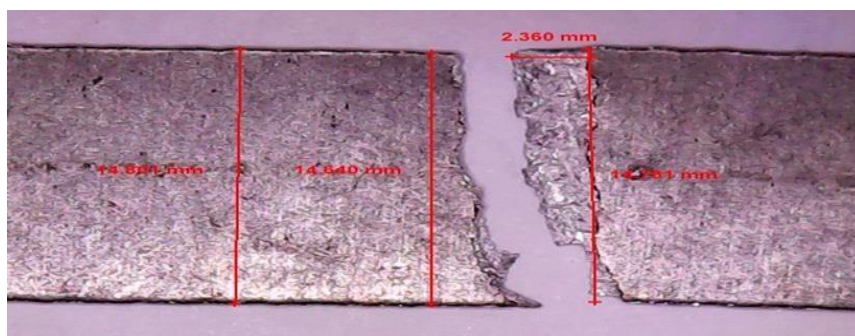


Figure 5.5. The tensile fracture mode of Mg AZ31 alloy.

The tensile specimen had three different uniaxial values, 16.844mm, 14.84mm, and 14.761mm, with 2.36mm punch length. We machined it out of AZ31 rods. We conducted a uni-axial tensile test on the specimen at a nominal strain rate of 1×10^{-3}

s⁻¹. In the rods' longitudinal direction, small punch and uniaxial tensile loading were carried out, as Figure 5.5 shows.

5.2. INVESTIGATION OF THE CUTTING FORCES THAT OCCURRED DURING THE PUNCHING PROCESS.

It is easy to understand that punch tips with different tip geometries cause stress distributions. We observed that the flat punch showed the highest punch force, and the P3 (16°) punch showed the lowest force. As explained in the previous pages, punch angle significantly affected the punch force because of the contact area-force relation. Lower forces were seen on the P2(R) punch, and the apparent difference is that the angle in the middle of the punch, which is P1(0°), and the contact area is more than the P3 (16°) punch, so the punch force is higher in the P1 (0°) punch. Shear forces obtained from punching operations done with Mg AZ31 alloy are given in Figure 5.6. for all punch geometries.

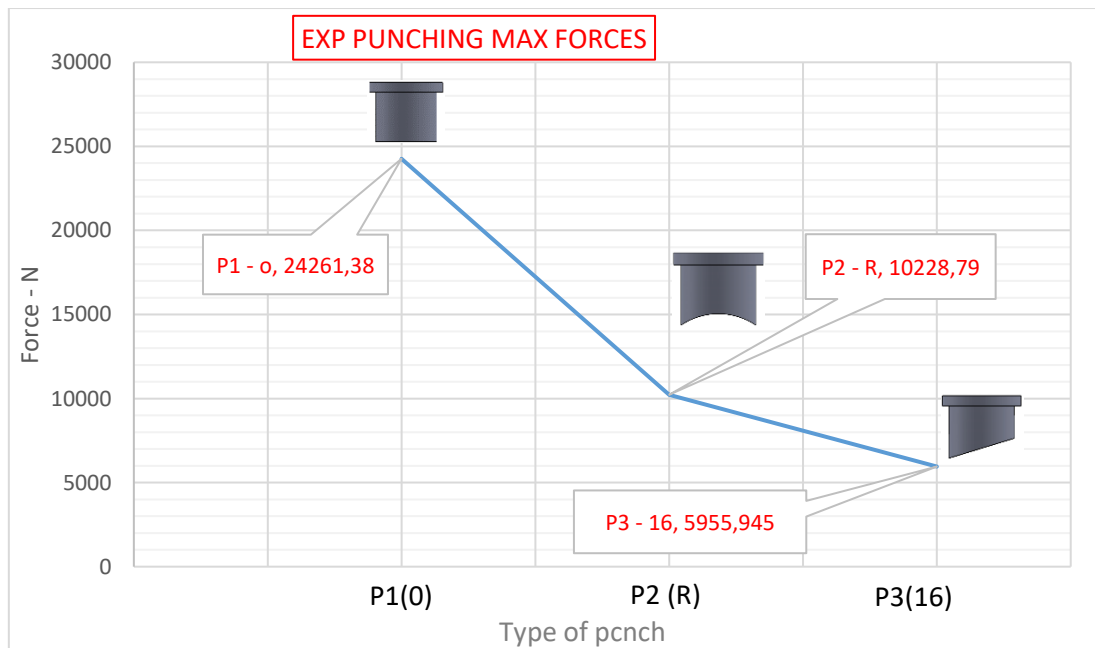


Figure 5.6. Mg AZ31 alloy cutting forces derived from punching for all punch geometries.

As shown in Figure 5.6, we used different punch geometries in punching processes with constant cutting speeds and a constant cutting gap. The shear force for Mg AZ31 alloy is in P1(0°) (24261.38). The cutting force for the P2(R) concave punch was 10228.79 N, and the cutting force for the P3 (16°) angled punch was 5955.945 N. Thus, in punching experiments using different punch geometries, we obtained the highest cutting force using P1 (0°) straight punch geometry while using the lowest cutting force with P3(16°) angled punch geometry. The P1 (0°) flat punch had the highest cutting force. Comparison of cutting forces was performed for P1 (0°), P3 (16°), and P2 (R), respectively. Fig. 5.7 and 5.8 show these comparisons.

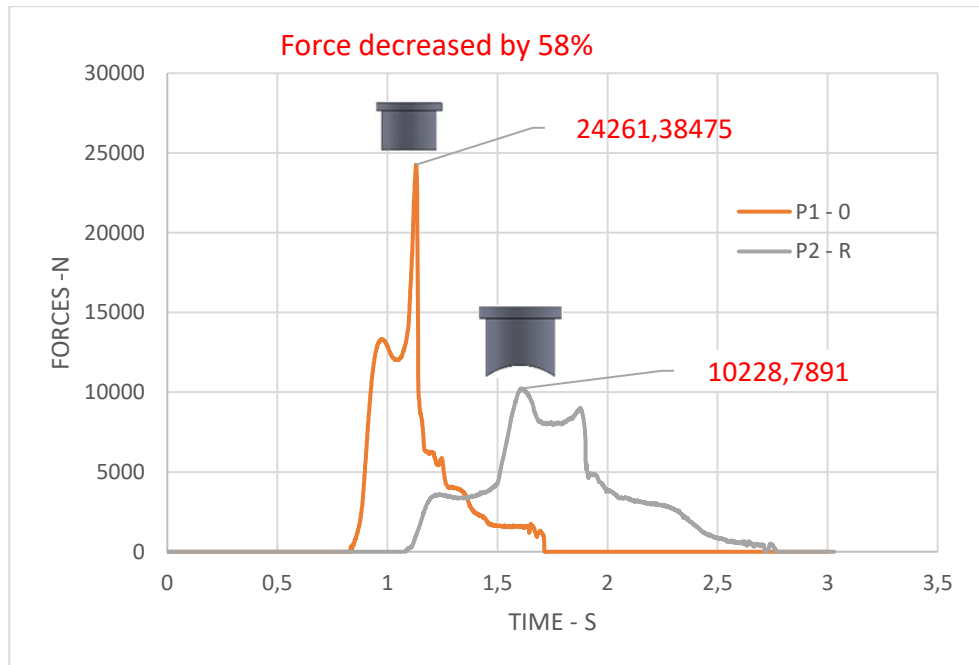


Figure 5.7. P1 (0°) flat punch versus P2(R).

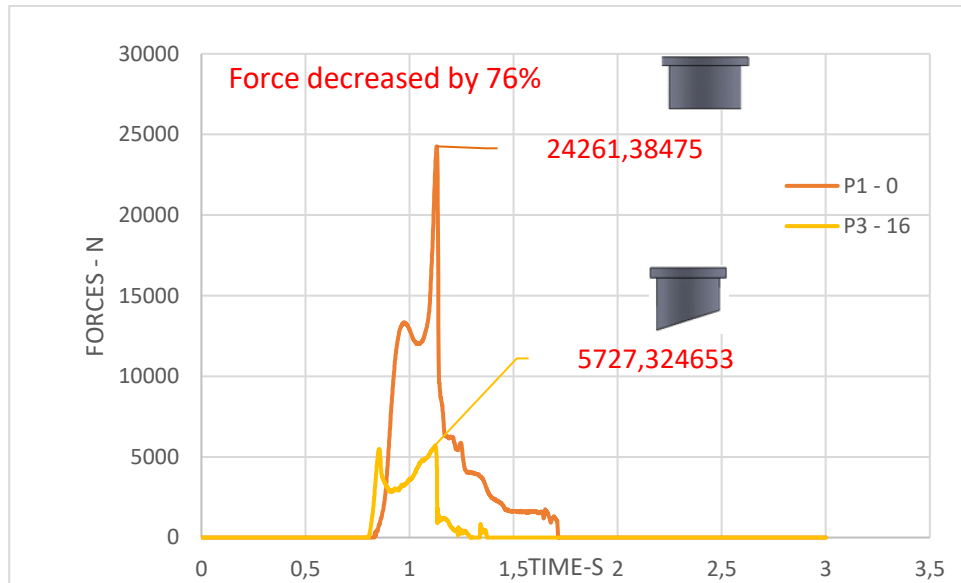


Figure 5.8. P1 (0°) flat punch versus P3 (16°) punch cutting force.

Figures 5.7 and 5.8 show that cutting forces are significantly low when using inclined punch geometries. Cutting forces decreased by 58% and 76% in punching processes, respectively, compared to flat-edged punches. We conducted the punching process of MgAZ31 alloy using punches, which had different geometries. Using P1 (0°), we noted the maximum cutting force, and it was the lowest when we used P2 (16°) angled punch geometry. We obtained the highest cutting force using straight punch geometry, but angled punches led to the lowest. Stapler mentioned in the same study that angled-inclined punch geometries reduce the cutting forces, which are reduced by 78% in comparison with straight punches [80].

5.2.1. Shear Force Analysis with FEM Software

Using FEM, we carried out different simulations and analyses. For consistency, 3D models were used to test the software performance for punching simulation. For research, we used 3D models for punching AZ31 alloys with P1 (0°) straight, P2 (R) concave, and P3 (16°) angled punches, shown in Figure 5.9. and 5.10.

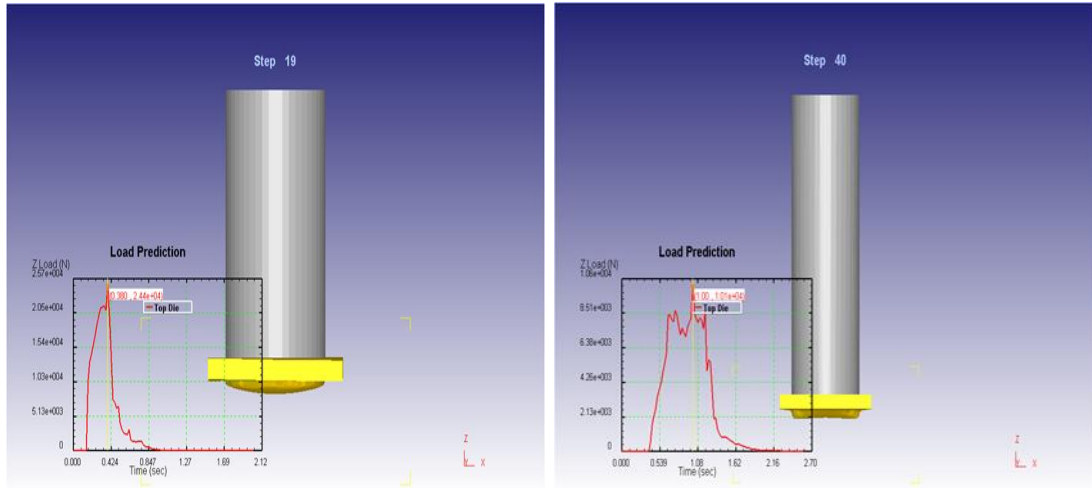


Figure 5.9. Results were obtained using the 3D model for punching P1 (0°) and P2 (R) punches of Mg AZ31 alloy.

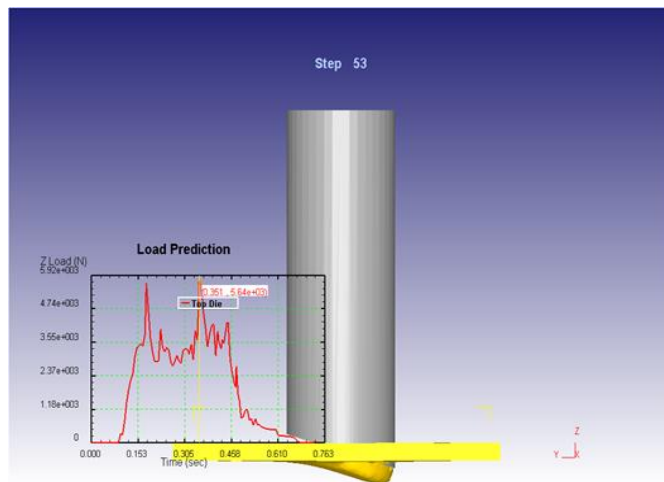


Figure 5.10. Results were obtained after using the 3D model for punching P3 (16°) punches of Mg AZ31 alloy.

The cutting force for the P1 (0°) flat punch using the finite element software was 2.4444 N. The cutting force obtained because of the experimental study was 2.4230 N. Similarly, 1.0132 N and 1.0229 N were observed for P2 (R) concave punch, and 0.5640 N and 0.5552 N for P3 (16°) angled punch. The first value belongs to the finite element analysis, and the second is the experimental study. Figures 5.11 and 5.12 show the results obtained from the finite element software and the experimental studies for the used punch geometries. Figure 5.13 shows a comparison between the cutting forces obtained from the finite element software and punching operations for Mg AZ31 for all the used punch geometries.

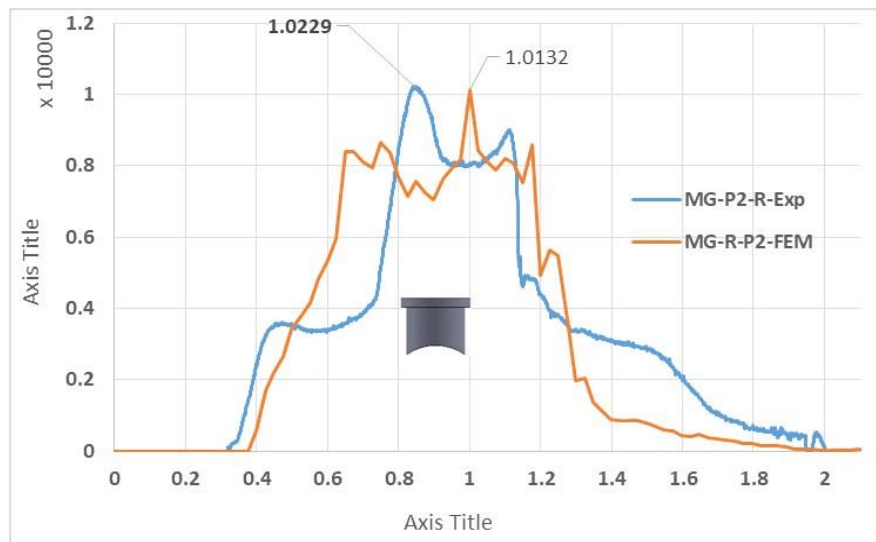
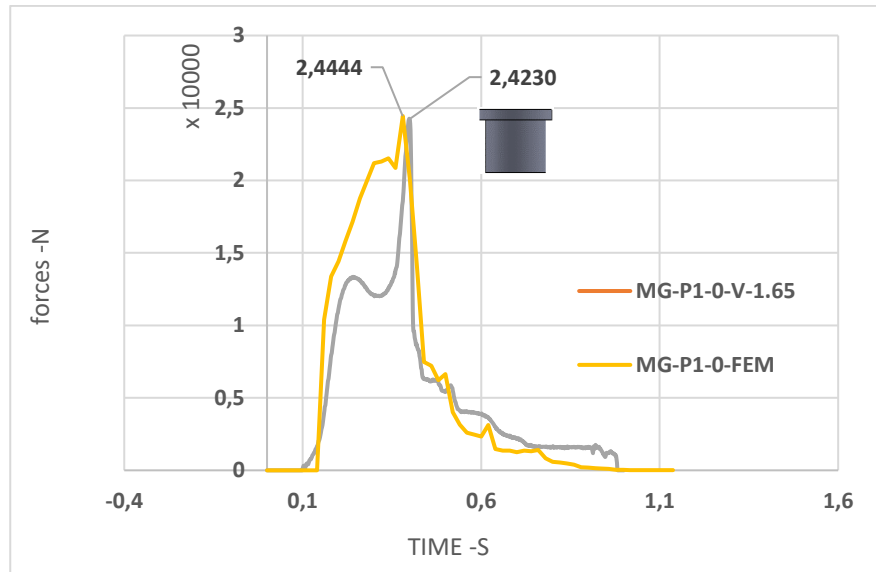


Figure 5.11. P1 (0°) straight punch and P2 (R) punch analysis and experimental study of cutting forces.

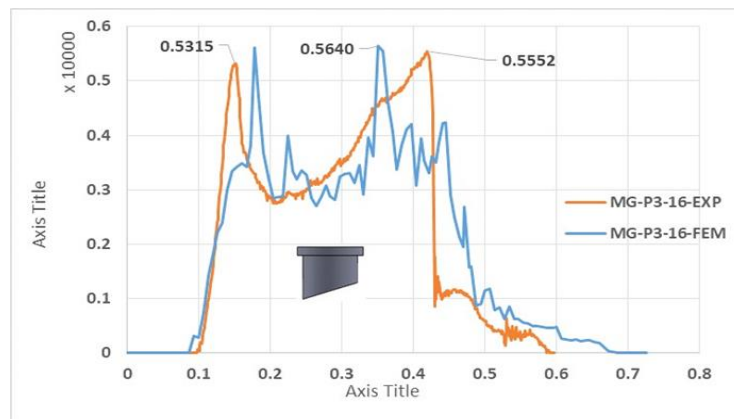


Figure 5.12. P3 (16) punch analysis and experimental study of cutting forces.

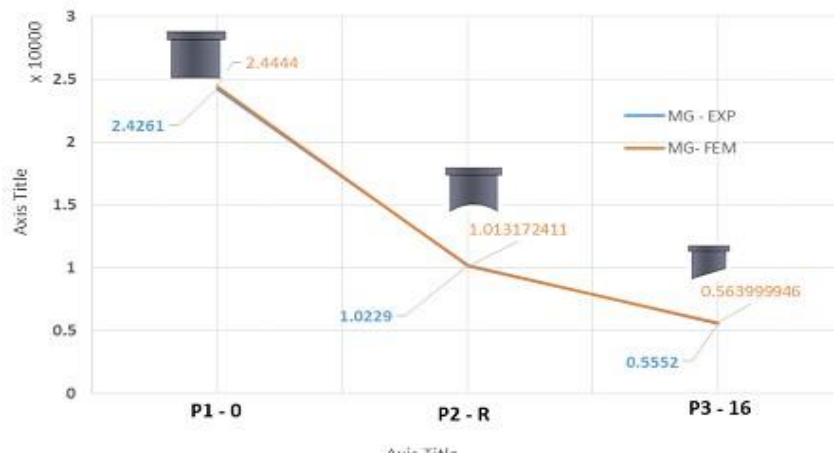


Figure 5.13. Comparison between cutting forces from the FEM and the punching operations for Mg AZ31 alloy.

5.3. MEASUREMENT OF THE DIMENSIONS OF PUNCHED PARTS



Figure 5.14. Dimensions of punch geometry (length 151.26mm, width 27mm).



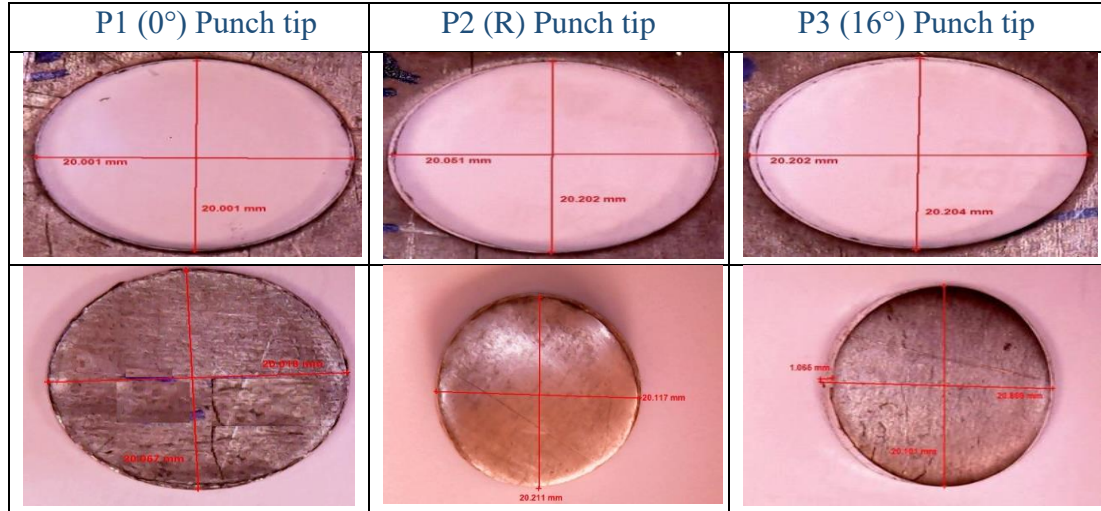
Figure 5.15. Dimensions of punches P1 (0°), P2(R), and P3 (16°).

5.3.1. Dimensional Analysis of Holes Created by the Punching Test

Significant differences occurred in the hole dimensions and blanking because of differences in the punch-tip geometries, as shown in Figures 5.16. Thus, we concluded that different insert hole-and-blank geometries of Mg AZ31 significantly affect the

dimensional accuracies of the hole and the blanking diameter. Table 5.1. shows Mg AZ31 alloy diameter values and display of damaged points.

Table 5.1. Mg AZ31 alloy diameter values and display of damaged points.



Figures 5.16 and 5.17 show changes in holes and blanks diameters after the Mg AZ31 metal sheet punching process for all punch geometries.

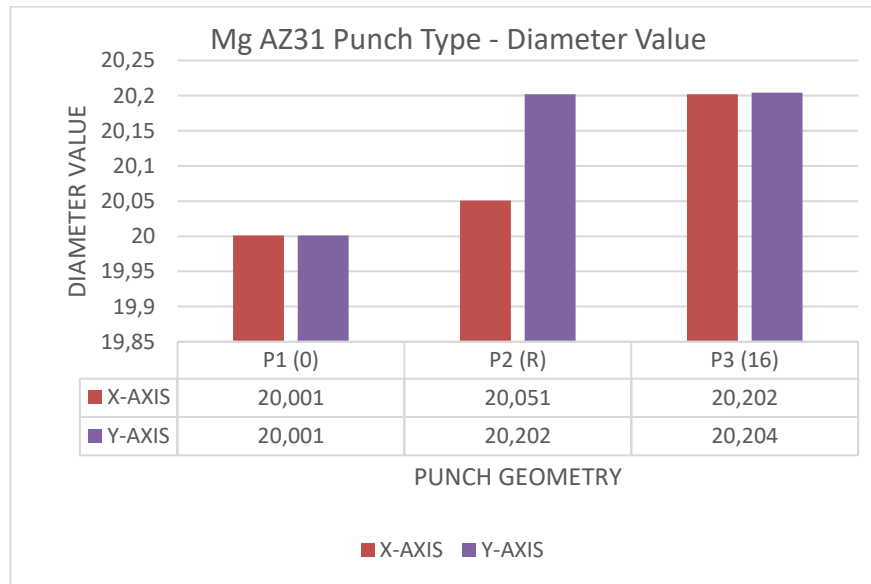


Figure 5.16. Hole diameters formed according to Mg AZ31 sheet metal's punch geometry.

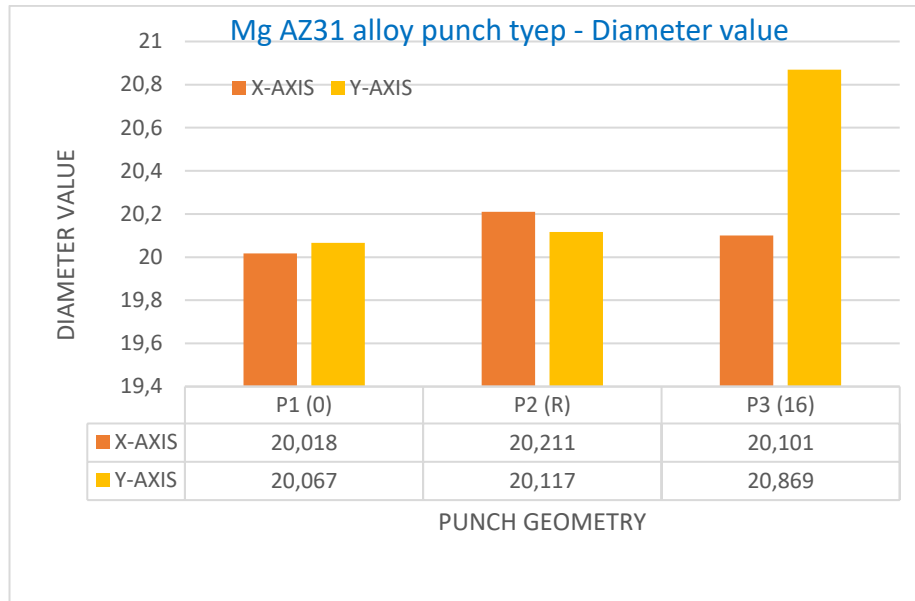


Figure 5.17. Blanking diameters formed according to Mg AZ31 sheet metal’s punch geometry.

Figures 5.16 and 5.17 indicate that the slightest deviation occurred for P1 (0°) for a flat-punch geometry. Automotive steels DP600 were used and with different hole geometries such as flat angle 0°, 4°, 16°, and concave R, where it was stated that the least deviation in hole diameter dimension occurs when using 0° flat punch. It was also mentioned in the same study that the geometric shapes for hole oblique and angular holes affect the accuracy of the hole diameter and create large differences in the accuracy of the dimensions of the hole diameter [81].

Top views of a hole and blank diameter of Mg AZ31 alloy sheet material punched with different punch geometries are shown in Figure 5.16. and 5.17, respectively. Damaged areas formed during the punching process are marked on the images. Thanks to the punch tip geometries, damaged areas are visible at the first contact points between the workpiece and the punch tips. Diameter measurements have been made. Size differences for all hole and blank geometries in Mg AZ31 alloy sheet material punching process are between $20^{+0,204}_{-0,001}$ for hole diameter and $20^{+0,869}_{-0,018}$ for blank diameter [86].

5.3.2. Diameter Deviations and Deviation from Circularity (Ovality)

The main goal is to obtain the ideal diameter hole in the punching operations. The diameter of the holes obtained by punching is affected by many parameters, such as punch geometry, cutting gap, cutting speed, and material strength. We investigated the effect of punch geometry on the diameter deviation. Figures 5.18 and 5.19 show the deviation values in the drilling process of Mg AZ31 alloy.

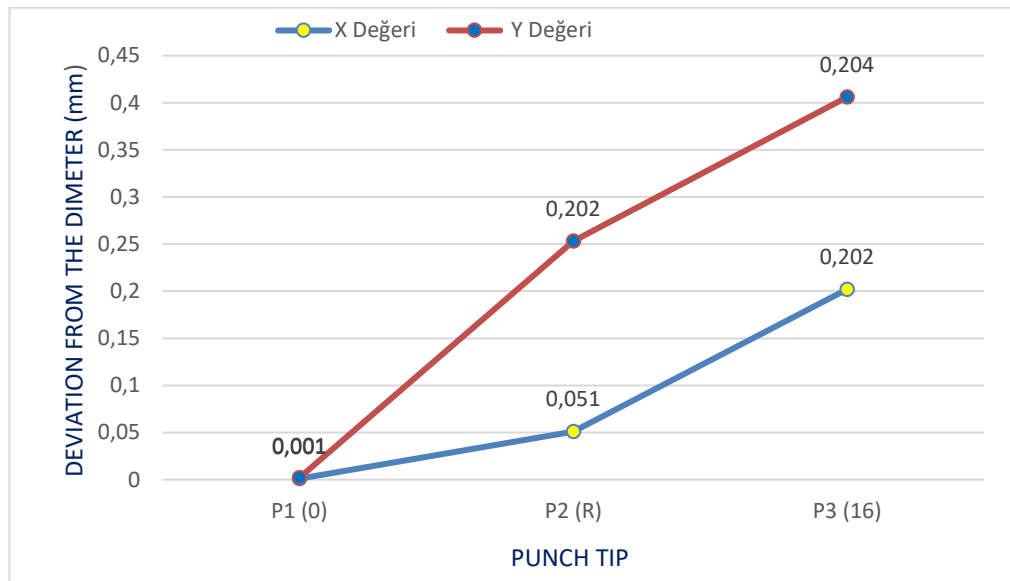


Figure 5.18. Diameter deviation for Mg AZ31 alloy punch geometry of the hole.

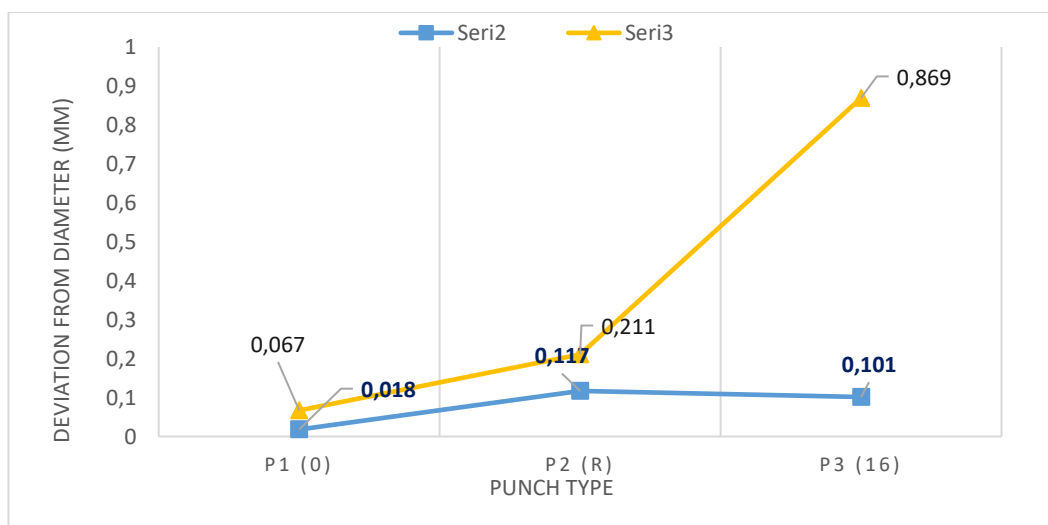


Figure 5.19. Diameter deviation for MgAZ31 alloy punch geometry for blanking.

The measurements in the hole of an AZ31 workpiece show that the deviation values from the diameter for all punch geometries were within the range of 0.001-0.202mm, and they varied within the range 0.067-0.869mm for blanking (scrap) of the Mg AZ31 alloy. Figure 5.20 shows the deviation values that occur in the punching process of a hole (workpiece) and blanking (scrap) of Mg AZ31.

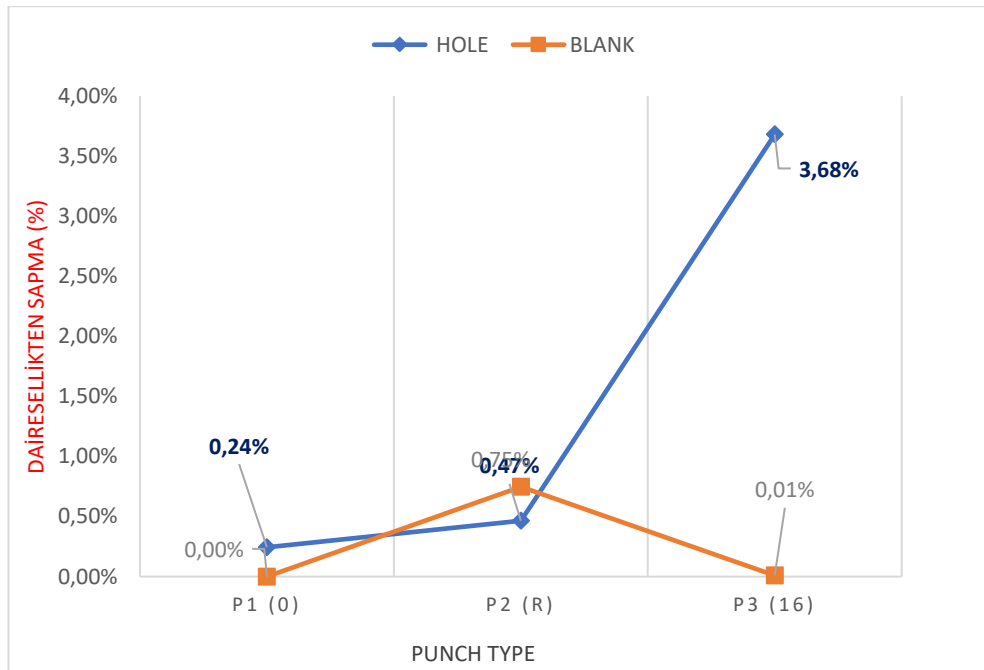


Figure 5.20. Deviation from the circularity of the hole (workpiece) and blanking (scrap) punch geometry.

First, the hole measurements (workpiece) were made, and the deviation values from the diameter for all punch geometries were within the range 0.24-3.68% for all punch geometries and 0.00-0.75% for all punch geometries the blanking (scrap) of the Mg AZ31 alloy.

5.3.3. Investigation of Cutting Surfaces Resulting from Punching Process by A Digital Microscope

In the punching process, the cutting surface consists of four different regions. The rollover region is the first that exists at the top of a cutting surface. This region corresponds to the indentation that the punch makes in the material before the cutting process, and here, the first plastic deformation occurs. A smoother and brighter part

appears immediately after rolling called burnish, which emerges just before the fracture. This region exists just below the brilliant part in the fracture zone. The fracture zone has a relatively rougher surface compared to the other zones. After the fracture, the metal elongation causes a sharp corner during the final separation of the two parts, which forms at the lowest edge of the material, and this part is called a burr [82]. We cut the Mg AZ31 samples in half from the axis with a saw after punching and examined them under a stereomicroscope to determine the regions of the cutting surface. For different cutting regions, we took measurements after the punching process. Table.5.2. shows the cutting surface images for Mg AZ31 alloy material.

Table 5.2. MgAZ31 alloy cutting surface image formed after drilling with a punch.

Measurements P1(0°) Cutting Surface	Measurements P2(R) Cutting Surface	Measurements P3(16°) Cutting Surface

Upon examination, P1 (0°) flat punch had the most homogeneous cutting surface in punching processes made with Mg AZ31 alloy. P1 (0°) straight, P2 (R) concave, and P3 (16°) angled cutting surface images were obtained during punching with punches with visible tip geometry, rollover, burnish region, fracture region, and burr formation (Table.5.2). When examined, various damages appeared in P2 (R) and P3 (16°) punch geometries, respectively, used in punching with Mg AZ31 alloy due to the high

stresses formed at the first contact points with the workpiece occurs. The rollover depth, burnish depth, fracture depth, and burr height are presented in Table 5.2. As a result of these damages, changes in the thickness and diameter of the workpiece occurred. The workpiece thickness in the damaged region decreased by 0.212mm when the P2 (R) geometry punch was used and by 0.473mm when the P3(16°) punch geometry was used.

Table 5.3. Rollover depth, burnish depth, fracture depth, and burr height.

Material	Punch Shape	Rollover depth, mm	Burnish depth, mm	Fracture depth, mm	Burr height, mm
Mg AZ31	P1(0)	0.222	1.722	1.297	0.192
Mg AZ31	P2(R)	0.219	1.376	1.719	0.129
Mg AZ31	P3(16°)	0.359	0.932	1.904	0.206

The comparison between rollover, burnish region, fracture region, and burr formation measurements for P1(0°), flat, P2 (R), and P3 (16°) punch geometries used in the punching process of Mg AZ31 alloy is given in Figure 5.21.

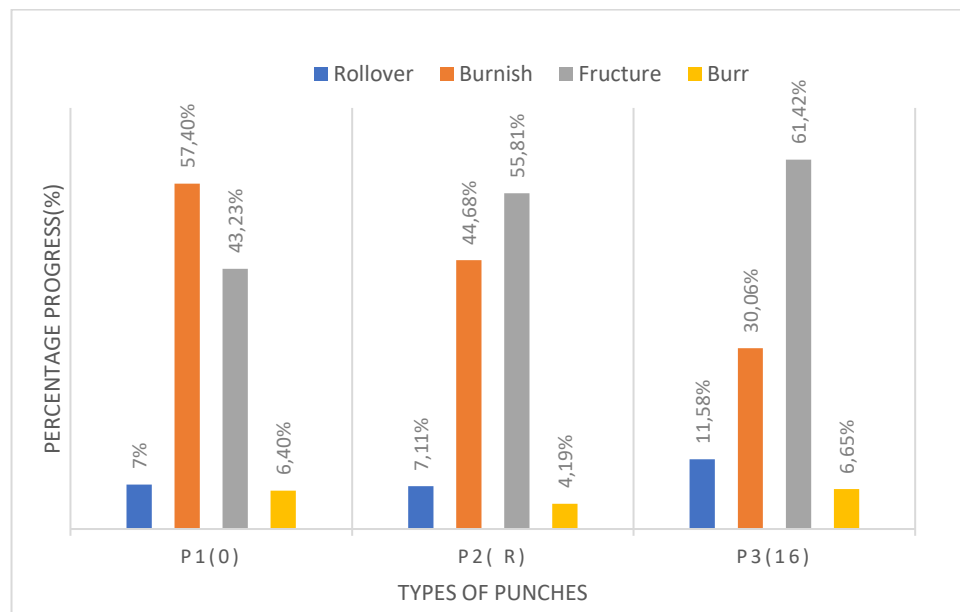


Figure 5.21. The cutting surface of Mg AZ31 alloy for all punch geometries.

The cutting surface properties affect the punched part's mechanical performance, so a large cutting region and smaller fracture region are needed to make a good cutting surface. Several factors affect the ratio of these regions, such as punch geometry, clearance, and material properties [79]. After performing the punching processes on an Mg AZ31 workpiece, the most homogeneous cutting surface occurred when we used P1 (0°) flat punch geometry (Figure 5.21). The cutting surface examination shows that 43.23% of the Mg AZ31 alloy thickness formation at the shearing region, 57.4% at the fracture region in P1 (0°), while in P2(R), it was 44.68%. It was 55.81% in the fracture region, the most expansive area compared to P1 (0°) and P3 (16°). Examination shows that for P3 (16°) angled punch geometry, the shearing region for Mg AZ31 alloy was 30.06% of the material thickness and 61.42% of the fracture region. We compared the mentioned values to other punch geometries, the widest shearing area and the lowest fracture region formed with flat punch geometry P1 (0°).


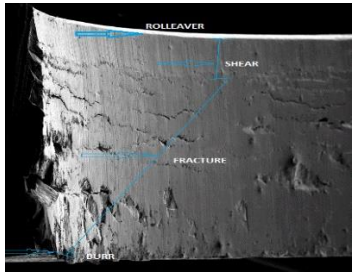
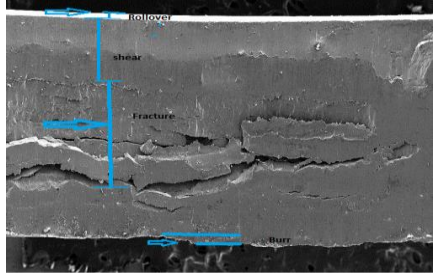
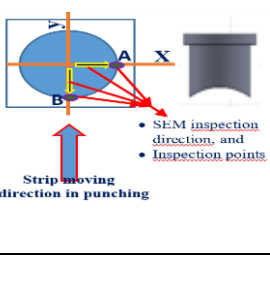
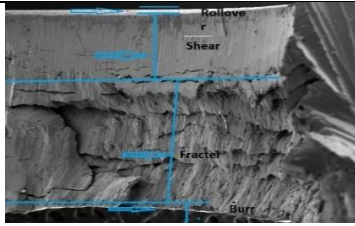
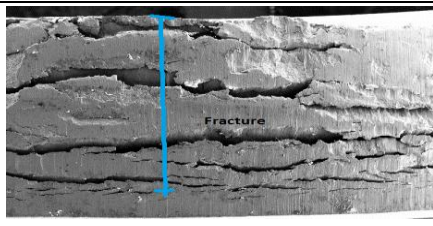
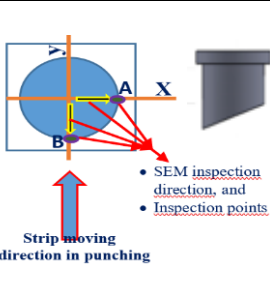
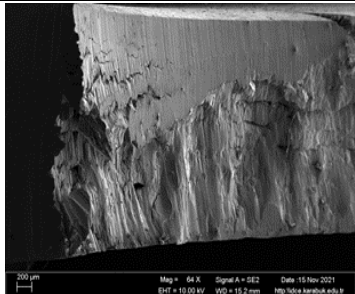
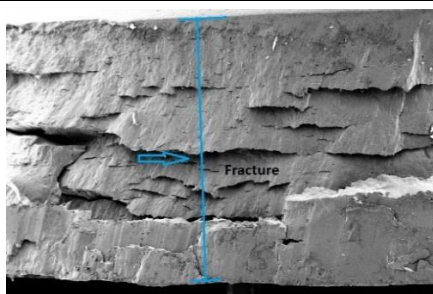
The flat punches are more efficient for proper form and dimensional accuracy with different punch geometries, such as 0° flat, 4°, 16°, and R concave for the DP600 automotive steel punching process [81]. When we obtained the cutting surface areas using P1 (0°) flat punch geometry of Mg AZ31 as compared to other punch geometries P2(R) and P3(16°), we noted that reduction in the inclination angle increases the shearing region and decreases the fracture area. Different hole shapes affect the stress distribution and fracture formation in the workpiece, and besides, materials undergo deformation when angled, and inclined punch geometries are used [81].

5.3.4. Investigation of Cutting Surfaces Resulting from Punching Process by Using SEM

The punched part's cutting surface images using SEM microscopy for Mg AZ31 helped analyze failures, presented in Table. 5.4. The photos show a sheared Mg AZ31 alloy's cross-sectional view. The cutting surface shows four regions: a burnish region, a rollover region, a burr region, and a fracture region. The rollover region is formed at the top of a cutting surface, while the burr region appears at the bottom. Inclining the clearance reduces the maximum trimming force because of a significant bend, essential for hydrostatic tensile stress in the shear region [83]. Moreover, increasing the negative







angle improves the sheared edge quality and reduces the shearing load. When the surface roughness increases, the burnish area increases while the fracture area reduces when the blade sharpness reduces. The cutting angle is a deciding factor that influences the rate of increase or decrease because it has an inverse relationship with the rate of increase/decrease. [84]. The rise in punch angle increases the deformation along the first and second deformation regions [85]. The examination of the Mg AZ31 cutting surface shows that the fracture region increased more when P2(R) and P3 (16°) as compared to P1 (0°). It means that when the angle increases, the fracture area rises, making the sample more brittle.

Table 5.4. Cutting surface images of Mg AZ31 taken by SEM.

Punches hole with axes, the photograph was taken a view and its points (A, B)	X-axis top view A point	Y-axis top view B point
 <ul style="list-style-type: none"> • SEM inspection direction, and • Inspection points <p>Strip moving direction in punching</p>		
 <ul style="list-style-type: none"> • SEM inspection direction, and • Inspection points <p>Strip moving direction in punching</p>		
 <ul style="list-style-type: none"> • SEM inspection direction, and • Inspection points <p>Strip moving direction in punching</p>		

One of the punching process's purposes is to focus on the falling part profiles, shown in Table 5.5 for all punch geometries.

Table 5.5. Side profile shapes of the falling parts were obtained by using different punches.

P1(0°) Flat Punch-tip Geometry	P2(R) Concave Punch Geometries	P3(16°) Angled Punch Geometry
		
		

The falling parts' profiles form when a punching process changes according to the punch-tip geometry. A P1 (0°) flat punch creates a properly-shaped residual piece, but a slightly deformed residual piece results from a P3 (16°) angled punch. P2(R) concave punch geometries result in a wholly distorted blanked part profile. The Mg AZ31 punching process formed the blanked part profile when using the P1 (0°) flat punch-tip geometry. Thus, angled punch-tip P3(16°) and concave punch-tip P2(R) geometries are not recommendable for Mg AZ31 if we need the residual punching part. The punches' cutting edge shapes negatively affect the falling parts' edge quality [85].

PART 6

CONCLUSIONS

In this research study, we used Mg AZ31 alloy because its usage areas have significantly increased in recent times. It has gained more importance in the manufacturing industry than ever before. A punching test on commercially obtained Mg AZ31 alloy and three punches with different cutting forces and tip geometries were tested and analyzed. FEM technology helped model the punching process in the experimental environment. Failure analysis techniques helped improve the cutting surface quality. Practical and theoretical examination of the punching processes of Mg AZ31 alloy is the primary goal of this study. After successful completion of the study, we derived the following conclusions from the results:

- After conducting punching experiments using three different punch-tip geometries, we observed the greatest cutting force using P1 (0°) flat punch. Contrary to that, the P3 (16°) punch showed the lowest punching force.
- It is clear from the observation that the punch tip geometry significantly affects the cutting force. The cutting force decreased by 58% in P1 (0°) flat versus P2 (R-V) and 76% in P1 (0°-V) flat versus P3 (16°-V) for Mg AZ31.
- The most uniform cutting surface existed when we performed punching with P1 (0°) for Mg AZ31 alloy.
- After experiments and FEM analysis, we found that the punching forces decreased because of the surface cutting angle in P2 and P3 punches.
- All three punching experiments (P1, P2, and P3) included the finite element method, and the observations show that the force values match the experimental force values.
- According to the findings, FEM is an effective simulation method that reduces costs, speeds up the industrial production process, and accurately predicts the blank products' cutting quality.

- The SEM's experimental study of the Mg AZ31 microstructure shows that the dark area shows a fracture, and microvoids appeared under three different magnification powers.
- The punching process for Mg AZ31 alloy showed deviations in the hole, blanking diameters, and material thickness losses with P2 (R) concave and P3 (16°) angle punch geometries.
- When we used SEM with an Mg AZ31 alloy sample, the cutting angle increases the fracture area and decreases the cutting area.
- SEM observations show that the Mg AZ31 cutting surface of Mg AZ31, the fracture region increases more with P2(R) and P3 (16°) as compared to P1(0°).
- The use of angled punches resulted in the deformity of the residual parts, which made them unusable after punching, so flat punch geometry P1 (0°) is recommendable to make the residual parts usable.

REFERENCES

1. Zhang, S. H., Cheng, S. U. N., & Wang, Z. T., "Finite element simulation on press forging of magnesium alloy AZ31 sheets", *Transactions of Nonferrous Metals Society of China*, 1(8): 269-272 (2008).
2. Easton, M., Beer, A., Barnett, M., Davies, C., Dunlop, G., Durandet, & Beggs, P., "Magnesium alloy applications in automotive structures," *Jom*, 60(11):57-62 (2008).
3. Priyanto, T. H., Insani, A., & Muslih, R., "Texture Analysis on the AZ31 Magnesium Alloy Using Neutron Diffraction Method", *In Journal of Physics: Conference Series*, 1(41): 12-61 (2020).
4. Sivanandini, M., Dhimi, S. S., & Pabla, B. S., "Formability of magnesium alloys," *Int. Journal of Modern Engineering Research*, 2(4): 67-91 (2012).
5. Chen, T. and Huang, B., "Formability of stamping magnesium-alloy AZ31 sheets," *J. Mater. Process. Technol.*, 142(3): 643–647 (2003).
6. Chen, F. K., Huang, T. B., & Chang, C. K., "Deep drawing of square cups with magnesium alloy AZ31 sheets", *International Journal of Machine Tools and Manufacture*, 43(15): 1553-1559 (2003).
7. Doege, E., & Dröder, K., "Sheet metal forming of magnesium wrought alloys—formability and process technology," *Journal of Materials Processing Technology*, 115(1): 14-19 (2001).
8. Palumbo, G., Sorgente, D., Tricarico, L., Zhang, S. H., & Zheng, W. T., "Numerical and experimental investigations on the effect of the heating strategy and the punch speed on the warm deep drawing of magnesium alloy AZ31", *Journal of Materials Processing Technology*, 191(3): 342-346 (2007).
9. Masoudpanah, S. M., & Mahmudi, R., "The microstructure, tensile, and shear Deformation behavior of an AZ31 magnesium alloy after extrusion and equal channel angular pressing", *Materials & Design*, 31(7): 3512-3517 (2010).
10. Chino, Y. "Enhanced room temperature formability of magnesium alloy sheets by suppression of basal texture formation," *in Journal of Physics: Conference Series*, 10(63):12-80 (2018).
11. Moosbrugger, C., "Engineering Properties of Magnesium Alloys," *ASM International*, USA, 56-78 (2017).

12. Shand, M. A., "The chemistry and technology of magnesia," *John Wiley & Sons*, USA, 45-67 (2006).
13. Dobrzański, L. A., Totten, G. E., & Bamberger, M., "The Importance of Magnesium and Its Alloys in Modern Technology and Methods of Shaping Their Structure and Properties," *In Magnesium and Its Alloys CRC Press*, 2(3): 67-89 (2019).
14. Song, G. L., & Atrens, A., "Corrosion mechanisms of magnesium alloys," *Advanced Engineering Materials*, 1(1): 11-33 (1999).
15. Luthringer, B. J., Feyerabend, F., & Willumeit-Römer, R., "Magnesium-based implants: a mini-review", *Magnesium Research*, 27(4): 142-154 (2014).
16. Czerwinski, F., "Magnesium injection molding," *Springer*, New York, USA, 135-145 (2008).
17. Internet: Emsley, J., "Magnesium," <https://edu.rsc.org/elements/magnesium/2020016.article/> (2021).
18. Dziubińska, A., Gontarz, A., Horzelska, K., & Pieśko, P., "The microstructure and mechanical properties of AZ31 magnesium alloy aircraft brackets produced by a new forging technology", *Procedia Manufacturing*, 2(3): 337-341 (2015).
19. Tomczak, J., Pater, Z., & Bulzak, T., "Thermo-mechanical analysis of a lever preform forming from magnesium alloy AZ31", *Archives of Metallurgy and Materials*, 5(7): 1211-1218 (2012).
20. Internet: Buymetal, B., "AZ31 Magnesium Sheet\Plate", <https://store.buy metal.com/magnesium/sheet-plate/az31.html/>(2021).
21. Khandelwal, A., Mani, K., Srivastava, N., Gupta, R., & Chaudhari, G. P., "Mechanical behavior of AZ31/Al₂O₃ magnesium alloy nanocomposites prepared using ultrasound-assisted stir casting", *Composites Part B: Engineering*, 12(3): 64-73 (2017).
22. Powell, B. R., Krajewski, P. E., & Luo, A. A., "Magnesium alloys for lightweight powertrains and automotive structures," *In Materials, Design and Manufacturing for Lightweight Vehicles*, 4(5): 125-186). (2021).
23. Catherine, L. D. K. and Hamid, D. A. "Mechanical Properties and Machinability of Magnesium Alloy AZ31 and AZ91—A Comparative Review," *In IOP Conference Series: Materials Science and Engineering*, 10(62):12-54 2021.
24. Blawert, C., Hort, N., & Kainer, K. U., "Automotive applications of magnesium and its alloys," *Trans. Indian Inst. Met*, 57(4): 397-408 (2004).
25. Internet: Hanusa, T. "Magnesium chemical element", <https://www.britannica.com/science/einsteinium/>(2021).

26. Yalınz, E., "Development of high temperature creep resistant aluminium-based sand cast magnesium alloys," *Master's Thesis, Middle East Technical University, Turkey, Ankara*, 56-67 (2018).
27. Loukil, N., "Alloying Elements of Magnesium Alloys: A Literature Review," *Web of Science*, 12(2): 34-57 (2021).
28. Arkhurst, B. M., Lee, M., & Kim, J. H., "Effect of resin matrix on the strength of an AZ31 Mg alloy-CFRP joint made by the hot metal pressing technique", *Composite Structures*, 20(1): 303-314 (2018).
29. Dziubińska, A., Gontarz, A., Dziubiński, M., & Barszcz, M., "The forming of magnesium alloy forgings for aircraft and automotive applications," **Advances in Science and Technology. Research Journal**, 10(31): 45-78 (2016).
30. Zhang, W., Zhang, H., Wang, L., Fan, J., Li, X., Zhu, L., Zhang, S., "Microstructure Evolution and Mechanical Properties of AZ31 Magnesium Alloy Sheets Prepared by Low-Speed Extrusion with Different Temperature", *Crystals*, 10(8): 644 (2020).
31. Liu, C., Liu, Y., Wang, Q., Liu, X., Bao, Y., Wu, G., & Lu, J., "Nano-Dual-Phase Metallic Glass Film Enhances Strength and Ductility of a Gradient Nanograined Magnesium Alloy," *Advanced Science*, 7(19): 200-1480 (2020).
32. Wu, G., Chan, K. C., Zhu, L., Sun, L., & Lu, J., "Dual-phase nanostructuring as a route to high-strength magnesium alloys," *Nature*, 545(7): 80-83 (2017).
33. Abbott, T. B., Easton, M. A., & Cáceres, C. H., "Designing with Magnesium: Alloys, Properties, and Casting Processes," *Handbook of Mechanical Alloy – Design*, USA, 487 (2004).
34. Wang, L., Li, Y., Zhang, H., Zhang, Z., Yang, Q., Zhang, Q., & Vedani, M., "Achieving enhanced plasticity of magnesium alloys below recrystallization temperature through various texture control methods," *Journal of Materials Research and Technology*, 9(6): 12604-12625 (2020).
35. Ulacia, I., Galdos, L., Esnaola, J. A., Larrañaga, J., Arruebarrena, G., de Argandoña, E. S., & Hurtado, I., "Warm forming of Mg sheets: From incremental to electromagnetic forming", *Metallurgical and Materials Transactions A*, 45(8): 3362-3372 (2014).
36. Huang, Z., Yang, G., Qi, C., Wang, R., & Shuai, M., "Shear Damage Suppression Model of Magnesium Alloy Plates," *Taiyuan University of Science and Technology*, China, 23-34 (2020).
37. Emonts, M. and Brecher, C. "Laser-assisted shearing of stainless steel and spring steel plates with the use of a laser scanner system-new hybrid production technology for the sheet metal industry," *Phys. Procedia*, 5 (3): 73–283 (2010).

38. Khan, A. S., & Huang, S., "Continuum theory of plasticity," *John Wiley & Sons*, USA, 12-19 (1995).
39. Liu, Z., "Numerical and experimental study of AZ31-O magnesium alloy warm sheet forming", Doctoral dissertation, *Ecole Nationale Supérieure des Mines de*, Paris, 67-78 (2012).
40. Zlitine, M. and Uporabe, P., "Magnesium alloys: a review of applications," *Magnesium*, 8(81): 890 (1999).
41. Agnew, S. R., & Duygulu, Ö., "Plastic anisotropy and the role of non-basal slip in magnesium alloy AZ31B", *International Journal of Plasticity*, 21(6): 1161-1193 (2005).
42. Fazily, P., Yu, J., & Lee, C.-W., "Characterization of Sheared Edges in Warm Blanking of Magnesium Alloy AZ31B", *Materials*, 12(7): 1023 (2019).
43. Internet: Mechanic, F., "Layout and Forming", www.flight-mechanic.com/layout-and-forming-part-seven/(2021).
44. Palumbo, G., Sorgente, D., & Tricarico, L., "Tangential bending and stretching of thin magnesium alloy sheets in warm conditions," *Materials & Design*, 30(3): 653–660 (2009).
45. Schumann, S., "The paths and strategies for increased magnesium applications in vehicles," *In Materials Science Forum Trans Tech Publications Ltd*, 48(8): 1-8 (2005).
46. Geiger, M., & Merklein, M., "Sheet metal forming-a new kind of forge for the future," *In Key Engineering Materials Trans Tech Publications Ltd*, 34(4): 9-20 (2007).
47. Internet: Design, S. "Difference between blanking, punching & piercing in sheet metal," <https://www.smlase.com/entries/sheetmetal-design/difference-between-blanking-punching-piercing/>(2021).
48. Zhang, G., Li, C., Zhou, H., & Wagner, T., "Punching process monitoring using wavelet transform based feature extraction and semi-supervised clustering," *Procedia Manufacturing*, 2(6):1204-1212 (2018).
49. Hoffman, H., "Metal Forming Handbook," *Springer Science & Business Media*, USA, 32-56 (1998).
50. Rajesh, G., "Modelling and simulation of stepper feeder mechanism for punch press," *Doctoral Dissertation, University of Mumbai*, India, 45-67 (2015).
51. Johanson, B., & Olsson, K., "Tooling solutions for advanced high strength steels," *In Uddeholm Automotive Tooling Seminar*, Austria, 12-23(2005).

52. Grigoras, C., Chirita, B., Brabie, G., & Ciofu, C., "Experimental analysis of AZ31B magnesium alloy sheet failure using punch stretching", *In IOP Conference Series: Materials Science and Engineering*, 682 (1): 12-19 (2019).
53. Fazily, P., Yu, J., & Lee, C. W., "Finite Element Analysis of Blanking Operation of Magnesium Alloy (AZ31) Sheet Using Ductile Fracture Criteria and Its Experimental Verification at Various Temperatures", *In Journal of Physics: Conference Series*, 1063(1): 12-158 (2018).
54. Xue, F., Yan, Y., & Kang, J., "Predicting forming limit diagrams for AZ31 magnesium alloy and 7050 aluminium alloy by numerical simulation", *The Journal of Strain Analysis for Engineering Design*, 56(8): 598-608 (2021).
55. Palaniswamy, H., Ngaile, G., & Altan, T. (2004). Finite element simulation of magnesium alloy sheet forming at elevated temperatures. **Journal of Materials Processing Technology**, 146(1): 52–60.
56. Chang, Q. F., Li, D. Y., Peng, Y. H., & Zeng, X. Q., "Experimental and numerical study of warm deep drawing of AZ31 magnesium alloy sheet", *International Journal of Machine Tools and Manufacture*, 47(4): 436-443 (2007).
57. Liu, D., Liu, Z., & Wang, L., "Simulation of the rolling process of AZ31 magnesium alloy sheet", **Procedia Engineering**, 8(1): 173-178 (2014).
58. Padmanaban, G., & Balasubramanian, V., "Optimization of laser beam welding process parameters to attain maximum tensile strength in AZ31B magnesium alloy", **Optics & Laser Technology**, 42(8): 1253-1260 (2010).
59. Zhou, M., Morisada, Y. and Fujii, H. "Effect of Ca addition on the microstructure and the mechanical properties of asymmetric double-sided friction stir welded AZ61 magnesium alloy", **J. Magnes. Alloy**. 8(1): 91–102 (2020).
60. Hekimoğlu, A. P., Çalış, M., & Ayata, G., "Effect of strontium and magnesium additions on the microstructure and mechanical properties of Al–12Si alloys", *Metals and Materials International*, 25(6): 1488-1499 (2019).
61. Jaafar, N. A., Abdullah, A. B., & Samad, Z., "Effect of punching die angular clearance on punched hole quality of S275 mild steel sheet metal", **The International Journal of Advanced Manufacturing Technology**, 101(5): 1553-1563 (2019).
62. Arslan, Y., & Özdemir, A., "Punch structure, punch wear and cut profiles of AISI 304 stainless steel sheet blanks manufactured using cryogenically treated AISI D3 tool steel punches", *The International Journal of Advanced Manufacturing Technology*, 87(1): 587-599 (2016).
63. Husson, C., Correia, J. P. M., Daridon, L., & Ahzi, S., "Finite elements simulations of thin copper sheets blanking: Study of blanking parameters on sheared edge quality," *Journal of Materials Processing Technology*, 199(3): 74-83 (2008).

64. Soares, J. A., Gipiela, M. L., Lajarin, S. F., & Marcondes, P. V. P., "Study of the punch–die clearance influence on the sheared edge quality of thick sheets," *The International Journal of Advanced Manufacturing Technology*, 65(4): 451-457 (2013).
65. Engel, U., & Eckstein, R., "Microforming—from basic research to its realization," *Journal of Materials Processing Technology*, 12(5): 35-44 (2002).
66. Vollertsen, F., Niehoff, H. S., & Hu, Z., "State of the art in micro forming," *International Journal of Machine Tools and Manufacture*, 46(11): 1172-1179 (2006).
67. Zhang, H., Zhang, C., Han, B., Qiu, J., Li, H., Qin, S. & Zhou, H., "Evolution of grain boundary character distributions in a cold-FEMed Nickel-based superalloy during electro pulsing treatment," *Journal of Materials Research and Technology*, 9(3): 5723-5734 (2020).
68. Colgan, M., & Monaghan, J., "The deep drawing process: analysis and experiment," *Journal of materials processing technology*, 132(3): 35-41 (2003).
69. Yoshihara, S., Manabe, K. I., & Nishimura, H., "Effect of blank holder force control in the deep-drawing process of magnesium alloy sheet," *Journal of Materials Processing Technology*, 170(3): 579-585 (2005).
70. Aminzahed, I., Mashhadi, M. M., & Sereshk, M. R. V., "Investigation of holder pressure and size effects in micro deep drawing of rectangular workpieces driven by a piezoelectric actuator," *Materials Science and Engineering: C*, 7(1): 685-689 (2017).
71. Luo, L., Jiang, Z., Wei, D., Manabe, K. I., Zhao, X., Wu, D., & Furushima, T., "Effects of surface roughness on a micro deep drawing of circular cups with consideration of size effects," *Finite Elements in Analysis and Design*, 11(1): 46-55 (2016).
72. Behrens, G., Trier, F. O., Tetzl, H., & Vollertsen, F., "Influence of tool geometry variations on the limiting drawing ratio in micro deep drawing," *International Journal of Material Forming*, 9(2): 253-258 (2016).
73. Dodd, B., & Bai, Y., "Adiabatic shear localization: frontiers and advances," *Elsevier*, Germany, 20-25 (2012).
74. Jiang, F., & Vecchio, K. S., "Hopkinson Bar Loaded Fracture Experimental Technique: A Critical Review of Dynamic Fracture Toughness Tests," *Applied Mechanics Reviews*, 62(6): 60-80 (2009).
75. Xu, J., Guo, B., Shan, D., Wang, C., Li, J., Liu, Y., & Qu, D., "Development of a micro-forming system for the micro-punching process of micro-hole arrays in brass foil," *Journal of Materials Processing Technology*, 212(11): 2238-2246 (2012).

76. Kurniawan, Y., Mahardika, M., & Suyitno, S., "The effect of punch geometry on punching process in titanium sheet", *Journal Technology*, 82(2): 23-45 (2020).
77. Liu, J., Gao, H., & Liu, H., "Finite element analyses of negative skin friction on a single pile," *Acta Geotechnica*, 7(3): 239-252 (2012).
78. Gürün, H., "The Experimental Investigation of Punching of the AM60 and AZ61 Magnesium Alloy Sheets by Using Varied Punch Shapes", *Journal of Engineering Research*, 12(3): 56-78 (2021).
79. Altan, T. ve Tekkaya, E., "Sheet metal forming: Processes and Applications," *ASM International*, Ohio, USA, 11-19 (2012).
80. Saier, A. A. E., "Theoretical and experimental investigation of punching process of DP800 automotive steel sheet with different punch tips", *Yüksek Lisans Tezi, Karabük Üniversitesi Lisansüstü Eğitim Enstitüsü*, Karabük, 12-32 (2021).
81. Ramah, M. M. M., "Theoretical and experimental investigation of the punching process of DP600 automotive sheet steel with different punch tips", *Yüksek Lisans Tezi, Karabük Üniversitesi Lisansüstü Eğitim Enstitüsü*, Karabük, 78-98 (2021).
82. Groover, M. P., "Principles of Modern Manufacturing," *Translation from the 4th Edition, Translation Editors Mustafa Yurdakul – Yusuf Tansel İç, Nobel Academic Publishing*, Ankara, 434-441 (2019).
83. H.-S. Choi, B.-M. Kim, and D.-C. Ko, "Effect of clearance and inclined angle on sheared edge and tool failure in trimming of DP980 sheet," *Journal of Mechanical Science and Technology*, 28(6): 2319-2328 (2014).
84. Li, M., "An experimental investigation on the cut surface and burr in trimming aluminium autobody sheet," *International Journal of Mechanical Sciences*, 42(5): 889–906 (2000).
85. Gürün, H., Göktaş, M., & Gültaş, A., "Experimental Examination of Effects of Punch Angle and Clearance on Shearing Force and Estimation of Shearing Force Using Fuzzy Logic," *Transactions of FAMENA*, 40(3): 19–28 (2016).
86. Yetgin, A., "Alüminyum 1100 ve Alüminyum 5005 serisi Sacların Farklı Zimba Uçları İle Delme İşleminin Teorik Ve Deneysel Olarak İncelenmesi", *Yüksek Lisans Tezi, Karabük Üniversitesi Lisansüstü Eğitim Enstitüsü*, Karabük, 42-68 (2021).

RESUME

Fadell ABOSHBA was born in Yefren, Libya, in 1978. He completed his early education in Yefren and later graduated from the Institute of Civil Aviation and Meteorology, Department of Aviation Engineering, specializing in Airframes and Engines in 2002. In 2008, he started working for Libyan Airlines. In 2020, he initiated his master's degree in Karabük University, where he studied at the Mechanical Engineering Department.